Soft Matter

PAPER

View Article Online
View Journal | View Issue

Cite this: *Soft Matter*, 2025, **21**, 3515

Quantifying and understanding the tilt of a Pt Janus active colloid near solid walls†

Jiayu Liu,‡[a] Yankai Xu,‡[b] Zihan Qiao,[a] Shanshan Li,[c] Xing Ma,[cd] Ting Kuang,[e] H. P. Zhang*[b] and Wei Wang*[a]

Received 21st January 2025,
Accepted 27th March 2025

DOI: 10.1039/d5sm00073d

rsc.li/soft-matter-journal

Active colloids powered by self-generated gradients are influenced by nearby solid boundaries, leading to their reorientation. In this study, the tilt angles (the angle between where an active colloid moves and where it faces) were measured to be 13.3° and −33.9° for 5 μm polystyrene microspheres half coated with 10 nm Pt caps moving in 5% H_2O_2 along the bottom and top glass wall, respectively, indicating that the colloids moved with their PS (forward) caps tilted slightly toward the wall. The speeds and tilt angles of Pt Janus colloids increased consistently with increasing H_2O_2 concentration (0.5 to 10 v/v%) and Pt cap thickness (5 to 50 nm). We propose that the tilt results from a balance between gravitational torque (caused by the Pt cap's weight) and chemical activity-induced torque (from self-generated chemical gradients), qualitatively supported by finite element simulations based on self-electrophoresis. Our findings are useful for understanding how chemically active colloids move in, and interact with, their environment.

Introduction

Chemically active colloids are particles that move directionally in a self-generated chemical gradient arising from asymmetric surface reactions.[1–4] Fundamentally, chemically active colloids serve as an effective model system for active matter,[5–7] an emerging field studying the collective behavior of self-propelled agents. On an applied level, they are used as prototypical microrobots by materials scientists and chemical engineers for applications ranging from biomedicine to environmental remediation.[8–10]

Whether used as a model for active matter or as a microrobot, a chemically active colloid typically moves along a solid surface, most likely a bottom wall, since the colloid is heavier than water and naturally settles. The presence of a solid boundary is known to significantly affect the speed, orientation, or trajectories of natural microswimmers.[11–13] Likewise, it has been shown both experimentally and theoretically that such boundaries significantly affect chemically active colloids, likely because of a complex interplay between chemical gradients, electrostatics, and hydrodynamics.[14–16] One consequence of the wall effect is the misalignment of the active colloid's motion relative to its orientation, resulting in a non-zero tilt angle (see definition below). The presence of such a tilt has important consequences. For example, in ref. 17 we showed that 2 μm polystyrene (PS) microspheres half coated with platinum (Pt) moving in hydrogen peroxide (H_2O_2) moved ∼146% faster when their tilts were rectified by alternating current (AC) electric or magnetic fields, so that they faced in the direction of movement. In a more recent study, we showed that the positive tilt angle is critical for a photocatalytically powered titanium dioxide (TiO_2)–Pt Janus colloid to be attracted to a solid boundary.[16]

Despite the significant influence of the tilt of a chemically active colloid on its dynamics near a wall, there is still a gap of knowledge in its origin and magnitude. On the experimental side, it has been sometimes reported that a chemically active colloid (for example, a microsphere half-coated with Pt moving in H_2O_2) moves with zero tilt, so that its Janus interface aligns perpendicularly to a solid wall.[12,18] Such an orientation is also sometimes assumed in studies that do not specifically focus on tilts.[15,19] On the other hand, several theoretical studies predicted based on diffusiophoresis that a chemically active colloid could move with a non-zero tilt.[20–22] This was experimentally confirmed in our own study of ref. 16 as well as a recent study by Carrasco-Fadanelli and Buttinoni,[23] yet the exact angle of tilt was not available. Nor has there been any

[a] School of Materials Science and Engineering, Harbin Institute of Technology (Shenzhen), Shenzhen 518055, China. E-mail: weiwangsz@hit.edu.cn
[b] School of Physics and Astronomy, Institute of Natural Sciences and MOE-LSC, Shanghai Jiao Tong University, Shanghai 200240, China. E-mail: hepeng_zhang@sjtu.edu.cn
[c] School of Integrated Circuits, Harbin Institute of Technology (Shenzhen), Shenzhen 518055, China
[d] Sauvage Laboratory for Smart Materials, School of Materials Science and Engineering, Harbin Institute of Technology (Shenzhen), Shenzhen 518055, China
[e] Education Center of Experiments and Innovations, Harbin Institute of Technology (Shenzhen), Shenzhen 518055, China

† Electronic supplementary information (ESI) available. See DOI: https://doi.org/10.1039/d5sm00073d

‡ Authors contributed equally.

systematic, experimental study of how this tilt varies with experimental parameters such as chemical activity and the cap weight of a Janus colloid.

Using Pt-coated Janus fluorescent polystyrene (PS) or silicon dioxide (SiO_2) microspheres moving in H_2O_2 as a model system, this study measures their tilt angles when moving along the bottom and top solid walls of an experimental chamber (sometimes referred to as the ''floor'' and ''ceiling'', see *e.g.*, ref. 22). In addition, we measure the change in their tilt angles when H_2O_2 concentrations (*i.e.*, chemical activity) and Pt coating thickness (*i.e.*, cap weight or bottom heaviness) were systematically varied. We also provide a qualitative explanation for the origin of the tilt and an estimate for its values using finite element simulations based on self-electrophoresis. This study advances the understanding and control of a chemically active colloid moving near solid boundaries, as well as in more complex environments, including liquid–liquid and liquid–air interfaces, obstacle-laden spaces, and dense populations.

Experimental

Materials and instruments

Hydrogen peroxide (H_2O_2, 30 wt%) was purchased from Alfa Aesar. Ethanol (CH_3CH_2OH, 99.5%) and isopropyl alcohol (C_3H_8O, 99.5%) were purchased from Aladdin, China. All chemicals were used without further purification. Fluorescent silica (SiO_2) microspheres were purchased from Tianjin Baseline Chromtech Research Center, China. Fluorescent polystyrene (PS) microspheres were procured from Shanghai Huge Biotechnology Co., Ltd of China. Glass cover slips coated with 200 ± 50 nm indium–tin oxide (ITO, custom-ordered) were subjected to 30-minute ultrasonic cleaning in ethanol and then isopropanol, followed by drying with nitrogen gas (N_2). Subsequently, they were subjected to 30-minute ultrasonic cleaning in deionized water (18.2 MΩ cm) and dried with N_2. The dried ITO were then stored in a dry glass container for future use. Green LED (THORLABS, M530L4) was used as to excite fluorescent light. A Leica EM ACE600 sputter coater was used to deposit platinum onto microspheres. A field-emission scanning electron microscope (FESEM; Zeiss SUPRA 55) was used for imaging. For the magnetic field experiment, a hand-held magnet was positioned near the experimental chamber.

Preparation of Janus microspheres

To make Janus microspheres, isotropic microspheres were suspended in 20 μL of ethanol and dispersed using ultrasound. Subsequently, the suspensions were deposited onto a small piece of clean silicon wafer to form monolayers. Janus active colloids, including SiO_2–Pt and PS–Pt were made by sputtering a layer of Pt of various thickness onto one side of the microsphere monolayers in a chamber prefilled with argon, at a vacuum level of 6.77×10^{-3} Torr with a high vacuum sputter coater (Leica EM ACE600). Following ref. 24, 5 μm PS–Ni–Pt Janus microspheres were made by evaporating a 15 nm Ni layer before sputtering Pt. The resulting Janus microspheres were dispersed in deionized water after sonication. Typical morphologies of the prepared Janus particles are shown in Fig. S1 (ESI†).

Experimental setup for observing and electrically manipulating Janus active colloids

The schematic of the experimental setup is shown in Fig. S2 (ESI†). The experimental chamber for AC experiments was constructed by stacking together 2 pieces of ITOs (10 to 15 Ω cm^{-2}), with the ITO sides facing each other. A silicone spacer ~400 μm thick (custom-ordered, Gracebio) was placed in between. A wave function generator (Keysight 33500B) was connected to both ITO slides with copper tapes, and sinusoidal waves of 10 V (peak to peak) and 1 MHz were applied. The 10 μL suspension of fluorescent Janus particles and 10 μL H_2O_2 with different concentrations of 1%, 2%, 5%, 10%, 20% were pipetted into the homemade chamber before the observation, to reach a final H_2O_2 concentrations of 0.5%, 1%, 2.5%, 5%, and 10%.

Data collection and analysis

An Olympus IX73 inverted fluorescence microscope and a Point Gray camera (GS3-U3-51S5C-C, Point Grey) were used for the microscopy and recording at 20 frames per second. The videos were processed and analyzed by MATLAB to yield the x–y coordinates of each colloid and their 2D instantaneous speeds. The 3D trajectories of the active colloids, especially their instantaneous positions along the z-axis, were obtained using the defocus-based algorithm (DefocusTracker) described in ref. 25. Additionally, MATLAB codes were developed to extract the fluorescence brightness of the particles for the subsequent calculation of the tilt angles.

The tilt angle (θ) of the fluorescent Janus active colloid was calculated from the brightness of the fluorescent micrographs (see Fig. S3 for schematic, ESI†). To elaborate, active colloids moving with different θ show distinct moon phases in the fluorescent micrographs. According to the literature,[26] θ can be calculated approximately

$$B = \frac{A}{2}(1 + \cos\theta)$$

where A is the fluorescence intensity of a Janus active colloid when θ is 90° (*i.e.*, the colloid is completely bright in the fluorescent micrograph, Fig. S3(i), ESI†), and B is the fluorescence intensity of a Janus active colloid with θ being studied (Fig. S3(ii), ESI†). In practice, the value A is hard to directly acquire from a fluorescence image, because a moving Janus active colloid is rarely completely bright. From previous studies,[27] we know that under an AC electric field, the Janus active colloid rectifies its tilt to minimize electrical energy. We therefore assumed that $\theta = 0°$ (corresponding to a half-moon phase) when an AC electric field is applied and doubled the intensity value obtained in this case to obtain A (Fig. S3(iii), ESI†). See the main text for the details of the AC electric field.

Numerical simulations

To elucidate the factors influencing the tilt angle of motors at the boundary, we utilize a 2D numerical model that solves the

Poisson–Nernst–Planck–Stokes equations.[28–35] This steady-state model operates under conditions of low Péclet and Reynolds numbers. The ion concentration fields are described by the Nernst–Planck equation: $\nabla\cdot\mathbf{J}_i = 0$ and $\mathbf{J}_i = -D_i\nabla c_i - z_i F\nu_i c_i\nabla\phi$, where $\mathbf{J}_i$ represents the ion flux, D_i the diffusivity, ν_i the mobility, z_i the valence, F the Faraday's constant, ϕ the electrostatic potential, and the subscript i indicates the ion species. The electrostatic potential is linked to the local free charge density through the Poisson equation: $-\varepsilon\nabla^2\phi = F\sum z_i c_i$, where ε is the permittivity of the liquid. Fluid dynamics are governed by the Stokes equations: $-\nabla p + \eta\nabla^2\mathbf{u} - \rho_e\nabla\phi = 0$ and $\nabla\cdot\mathbf{u} = 0$, where p is the pressure and $\mathbf{u}$ is the fluid velocity.

The model is driven by chemical reactions occurring on the motor surface. We impose a proton flux ($-J$) perpendicular to the boundary, directed inward near the poles of the Pt shell, while at the equator, the proton flux is directed outward. On the inert surface, the proton flux is zero, and the total proton flux across the entire motor surface is balanced to zero; other ion fluxes are also set to zero. At the particle surface, we apply the no-slip condition for fluid velocity and specify the local surface potential as $\phi = \zeta_m$. On the wall, chemical fluxes are zero, the electrostatic potential is set to $\phi = \zeta_w$, and the no-slip condition is enforced. At the outer boundaries of the computational domain, we set the potential and flow velocity to zero, and the ion concentrations to their bulk values, $c_i = c_{bulk,i}$.

We employ a finite-element method to solve the model. From the solutions of the physical fields, the electrostatic and hydrodynamic forces and torques acting on the motor are computed using the Maxwell stress tensor σ_E and the hydrodynamic stress tensor σ_H. The total force and torque on the motor, $\mathbf{F}_{tot}$ and $\mathbf{T}_{tot}$, are determined by combining these results with external force and torque arising from gravity. An iterative procedure is designed to identify the equilibrium state parameters of the forces acting on the motor at the boundary by adjusting V, θ, and h to minimize the magnitudes of the total force $|\mathbf{F}_{tot}|$ and torque $|\mathbf{T}_{tot}|$. The procedure terminates when $|\mathbf{F}_{tot}|$ and $|\mathbf{T}_{tot}|$ fall below a predefined threshold. For further details on the model, please refer to the ESI.†

Results

Chemically active colloids were prepared by half-coating 5 μm PS or 2 μm SiO_2 fluorescent microspheres with a thin layer of Pt (thickness varied from 5 to 200 nm, see below) by vacuum sputtering. See Fig. S1 (ESI†) for the scanning electron micrographs and elemental mapping of the prepared Janus microspheres. In a typical experiment, a dilute suspension (2D packing fraction $\phi = 0.06\%$) of 10 nm Pt Janus colloids in 5 v/v% H_2O_2 was placed on the surface of a pre-cleaned, hydrophilic glass slide and sealed at the sides and top to form an experimental chamber of 400 μm in height. See Fig. S2 (ESI†) for a schematic of the experimental setup. Due to gravity, these colloids sedimented to the bottom of the chamber and onto the surface of the glass slide (*i.e.*, the "bottom wall" of the experimental chamber), where they self-propelled toward the uncoated cap by the catalytic decomposition of H_2O_2 into water and O_2 on the Pt cap.[36] Results from PS–Pt colloids will be described in detail in the following, while the results from SiO_2–Pt colloids were qualitatively the same and can be found in the ESI† (Fig. S9 and Video S6).

Our key observation is that both the PS–Pt and SiO_2–Pt colloids moved near a solid wall with a non-zero tilt angle (θ), also known as the polar angle.[11] The tilt angle θ is defined in this work as the angle, measured clockwise, between the horizontal axis on the wall and the line connecting the centers of the two caps of the Janus colloid (see Fig. 1a for a schematic). Following this definition, a positive θ along the bottom wall means that the Pt Janus colloid moves with its uncoated/unreactive PS or SiO_2 cap tilted toward the wall, and that a negative θ means that the uncoated cap tilts away from the wall. The cases are opposite for colloids moving along the top walls, *i.e.*, negative θ corresponds to heads tilting toward the wall. Note that other definitions of θ have been used in the literature, for example setting $\theta = 0$ for a Janus sphere that points its Pt cap straight away from the wall[11,12,20,37] (corresponding to $\theta = 90^\circ$ in our definition), but this difference in definition does not affect our conclusions.

To quantify θ, one naturally turns to the partially transparent image obtained under optical microscopy, since the Pt cap blocks the transmitted light for a Janus colloid. However, it was difficult to distinguish the case of positive or negative θ with bright field transmission microscopy because the Pt cap would block the same amount of light and the micrographs would be indistinguishable in both cases (see Fig. S4 for schematic, ESI†). An example is given in Fig. S5 (ESI†), where the tilt angles were the same for two Janus magnetic colloids orientated differently with magnetic fields. To solve this issue, we used fluorescent PS or SiO_2 microspheres so that a "head down" colloid (*i.e.*, positive θ, its uncoated cap pointing toward the wall) would be bright for most of its circular projection when observed from below (Fig. 1b-ii, known as "gibbous" in the terminology of the moon phase). On the other hand, a "head up" colloid (negative θ, with the uncoated cap pointing away from the wall) would be partially illuminated only at the edge of the sphere (*i.e.*, crescent in the moon phase) when observed from the below. The value of θ can then be calculated from the fluorescence intensity of the moon phases (see Methods for calculation details). This technique of inferring the orientation of a Janus, fluorescent microsphere from its moon phase has been reported before (*e.g.*, ref. 38 and 39). It has also been used in a few experimental studies of chemically active colloids,[11,18,23,40,41] but tilt angles were not examined carefully or reported in these references.

In addition to the use of moon phases, for more accurate identification and calculation of θ, an alternating current (AC) electric field was applied across the thickness of the experimental chamber (see Fig. S2 for a schematic of the setup, ESI†). The electric field forced the half-dielectric, half-metallic colloid to orient with its Janus interface parallel with the electric field lines (and thus perpendicular to the wall) in order to minimize the electrical energy.[27] We set $\theta = 0^\circ$ in such case as the

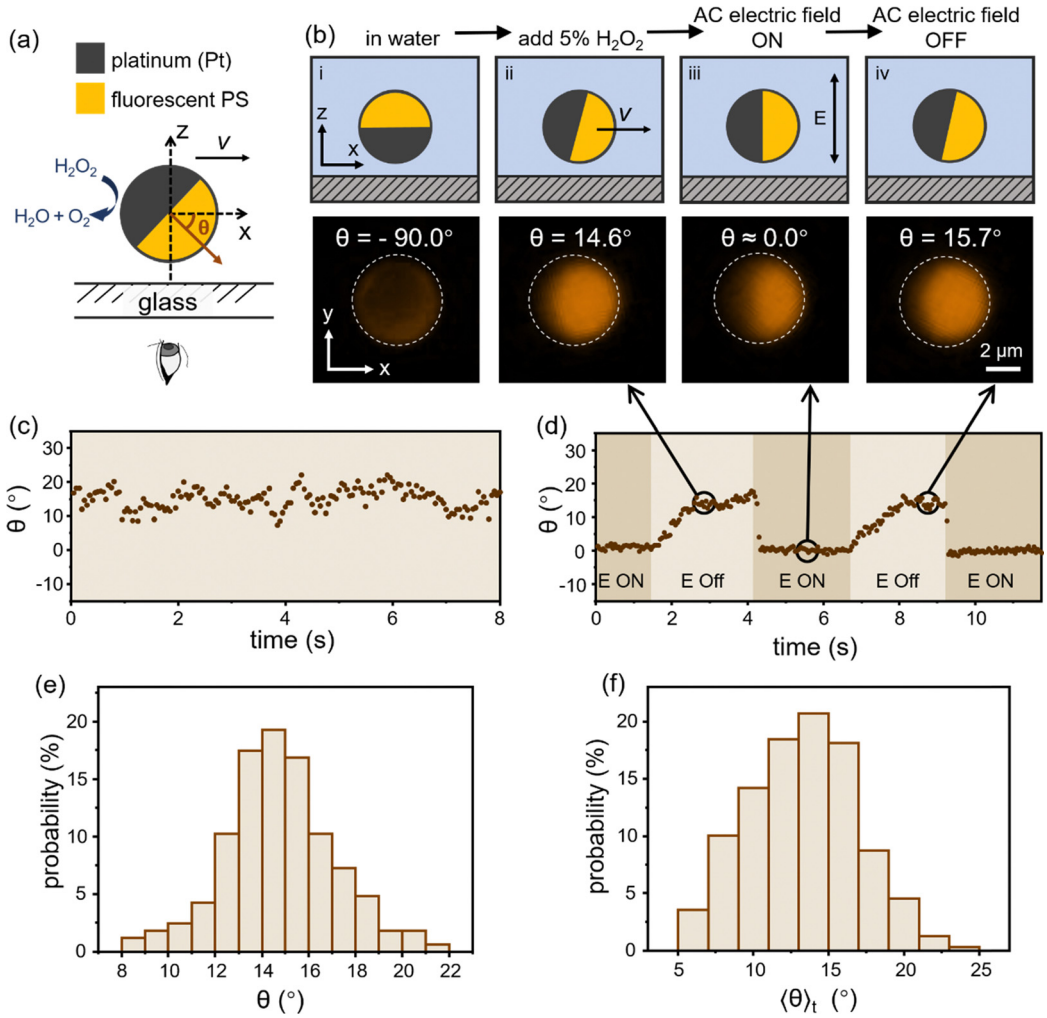

Fig. 1 Quantifying the tilt angles (θ) of Pt Janus active colloids moving along a glass bottom wall. (a) Schematic of the system, where the Pt cap on a fluorescent polystyrene (PS) microsphere catalytically convert H_2O_2 into water and O_2. The Janus sphere thus self-propels at a speed V along a glass bottom wall with a tilt angle θ defined according to the scheme. (b) Cartoon schematic (top row, side view) and the corresponding fluorescent micrographs (bottom row, bottom view) of a 10 nm Pt-coated PS microsphere initially settled to the bottom (i), activated by the addition of 5% H_2O_2 (ii), and in the presence (iii) or absence (iv) of a 1 M Hz AC electric field. See Videos S1 and S2 (ESI†). (c) and (d) The instantaneous θ of one 5 μm Pt–PS in 5% H_2O_2 along the bottom wall in the absence (c) or in the presence (d) of intermittent AC electric fields. Arrows connect the bottom-view fluorescent micrograph in (b) to the corresponding time stamps in (d). (e) Probability distributions of θ of one 5 μm Pt–PS in 5% H_2O_2 along the bottom wall over the course of ~10 seconds. (f) Probability distributions of the time-averaged θ ($\langle\theta\rangle_t$) of 100 5 μm Pt–PS in 5% H_2O_2, each averaged over ~5 seconds. The average and standard deviations of the data in (c), (e) and (f) are 15.1° ± 3.0°, 13.7° ± 1.9° and 13.3° ± 3.6°, respectively.

reference, and ignore the slight deviations that arises from the torque by gravity.[42] A similar strategy was used in ref. 42 to find the reference values of the fluorescence intensities of different moon phases of Janus particles, using a magnetic field instead of an electric field.

Using a combination of fluorescent particles and AC electric fields, we found that $\theta = -90°$ for a PS–Pt colloid sedimented to the bottom wall of the experimental chamber in the absence of H_2O_2 (Fig. 1b-i). In other words, the Pt cap pointed completely towards the wall, because the Pt cap was much heavier (density = 21.45 g cm^{-3}) than the PS cap (density 1.05 g cm^{-3}) and water. However, when 5% H_2O_2 was added, the PS–Pt colloid reoriented (over a period of ~3 s, see Fig. S6 and Video S2, ESI†) so that its Pt cap flipped upward. As an example, Fig. 1c shows such a PS–Pt colloid move along the bottom wall at a speed of 3.8 ± 0.68 μm s^{-1}, with its PS cap slightly tilted downward at an average θ = 14.6° ± 3.8° (the ± corresponds to the standard deviation over 8 s). However, its tilt was rapidly (in less 1 s) rectified (θ = 0°), and the motor speed increased to 6.5 ± 0.5 μm s^{-1}, upon the application of a sinusoidal AC electric field of 1 MHz and a time averaged electric field strength of 17.7 V mm^{-1} (*i.e.*, 10 V_{p-p} across a solution of 400 μm in thickness). When the AC field was turned off, the colloid gradually returned over a few seconds to θ values fluctuating by about ~15° with propulsion speeds around 4.0 μm s^{-1}. This process was repeated several times in Fig. 1d to show that the tilting of a PS–Pt colloid was highly reproducible. Finally, Fig. 1e and f show the distributions for the θ of one particular PS–Pt colloid over a period of operation (Fig. 1e), or for the time averaged θ ($\langle\theta\rangle_t$) of a population of PS–Pt colloids (Fig. 1f). These variations in θ are

possibly due to thermal noise, or the intrinsic inhomogeneity in the shape, size and coating of different PS–Pt colloids. Unless otherwise specified, all the θ values reported below are $\langle\theta\rangle_t$ for a population.

We show in Fig. S7 (ESI†) that such AC fields moved the PS–Pt colloids at $\sim$1 μm s^{-1} toward the Pt cap as typically found in the literature,[17] but all the values of colloidal speeds reported in this study were measured when AC fields were turned off to eliminate the AC-induced propulsion. Also note that immotile PS–Pt colloids of $\theta \sim -90^\circ$ because of H_2O_2 depletion resumed their tilt angles of 10–15° when H_2O_2 was replenished.

In addition to the bottom wall, a PS–Pt or SiO_2–Pt colloid is also able to move against gravity and along the top wall of an experimental chamber (Video S3, ESI†). On the top wall, they move with a θ that was non-zero but different from that on the bottom wall. To elaborate, experiments were performed with the same 5 μm PS–Pt Janus colloids in 5% H_2O_2, in the same experimental chamber, as described above. The PS–Pt colloids were made to move on the top wall in one of two ways. Because the Pt cap was heavier, some Janus colloids spontaneously lifted off the bottom when H_2O_2 was added (or upon perturbations), moved through the bulk liquid against gravity, and reached the top wall along which they continued to move. Similar observations have been reported previously,[22] except that SiO_2–Pt colloids were able to move along the top wall ("ceiling") in our experiments, while ref. 22 reported that they could not. Alternatively, the experimental chamber could be flipped so that those originally moving along the bottom wall were at the top after flipping. These active colloids would not disengage from the top because of an activity-induced attraction between the colloid and the wall that counteracted gravity. The details of this wall-induced attraction are given in a recent study of ours,[16] but are not relevant to the current study.

Along the top wall, PS–Pt colloids moved at a tilt angle (θ_{top}) of $\sim -33.9^\circ \pm 4.8^\circ$ (± represents the standard deviation of $\sim$100 colloids), suggesting that they also moved with their PS caps toward the wall (Fig. 2g and Fig. S8, ESI†). The PS–Pt colloids moved against gravity and through the bulk liquid at a speed of 5.9 ± 1.8 μm s^{-1} (± corresponds to the standard deviation over 4 s of one same PS–Pt colloids). After correcting for the downward sedimentation velocity due to gravity (estimated to be 2.7 μm s^{-1}, see the caption of Fig. 2 for details), the

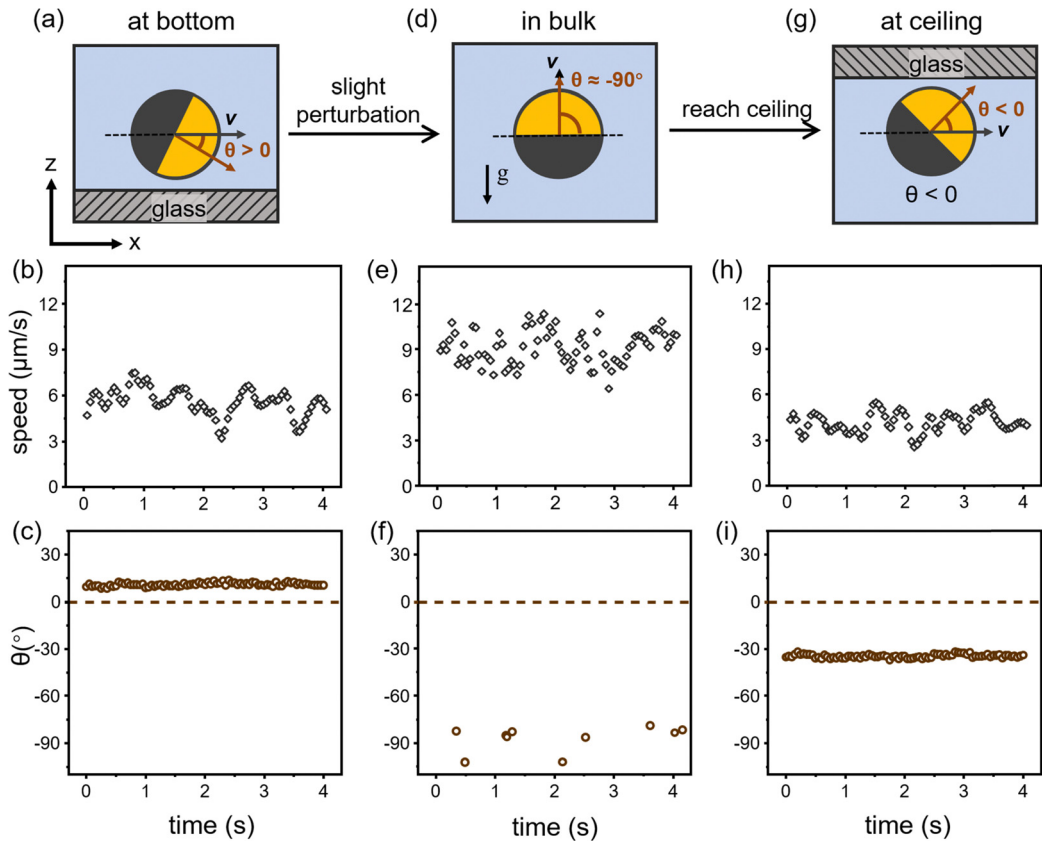

Fig. 2 The speeds and tilt angles (θ) of 5 μm Pt Janus active colloids (10 nm Pt coating) when swimming near the bottom wall (a)–(c), in the bulk liquid (d)–(f) and near the top wall (g)–(i). Instantaneous values of one representative active colloid are given in (b)–(i). The average and standard deviations are 5.6 ± 1.0 μm s^{-1} (b), 10.8 ± 1.0° (c), 8.6 ± 1.8 μm s^{-1} (e), −87.3 ± 7.8° (f), 4.1 ± 0.7 μm s^{-1} (h), −33.9 ± 1.2° (i). The upward speeds in (e) was obtained by summing the experimentally measured upward colloidal speed V with its theoretical sedimentation speed $V_t = 2(\rho_p - \rho_w)a^2g/9\eta$, where ρ_p and ρ_w is the density of the Janus particle and water respectively, a is the particle radius, g is 9.8 m^2 s^{-1}, and η is the viscosity of water at 298 K. The 3D trajectory of the active colloid was obtained using the defocus-based algorithm (DefocusTracker).[25] Note that the θ values in (f) and (i) are negative according to our definition for a Janus colloid tilted to the ceiling.

effective self-propulsion speed in the bulk was 8.6 ± 1.8 μm s^{-1}, higher than the speed along the bottom wall (5.6 ± 1.0 μm s^{-1}) and that along the top wall (4.1 ± 0.7 μm s^{-1}). One intuitive explanation for such speed differences between different swimming environments is the difference in their tilt angles: the propulsive force of an active colloid swimming in the bulk against gravity was almost entirely aligned with its swimming direction, but only a fraction of the propulsive force contributed to the motion when it moved along the bottom or top wall because of a non-zero tilt. The more the propulsive force deviated from its swimming direction, the slower a PS–Pt colloid moved, an effect we called "tilt-induced retardation" in ref. 17. Note that although the data above and in ref. 17 suggest that a larger tilt is correlated with a smaller propulsion speed, the causal relationship is not clear, given the complex interplay among the electrical fields, chemical gradients and hydrodynamics at the boundary.[16] Also note that our results are different from ref. 23, which showed that Pt coated active colloids moved at approximately the same speeds regardless of whether near a bottom or a top wall.

We also discovered that θ along the bottom wall was sensitive to the H_2O_2 concentration (Fig. 3a and b) and the thickness of the Pt cap (Fig. 3c and d) of a PS–Pt colloid. The data in Fig. 3a show that 5 μm PS–Pt colloids of 10 nm Pt cap moved along the bottom wall progressively faster from 1.8 ± 0.8 to 5.7 ± 1.3 μm s^{-1} when the H_2O_2 concentration was increased from 0.5% to 10%. At the same time, Fig. 3b shows that θ increased from $5.2 \pm 1.6^\circ$ to $15.2 \pm 3.6^\circ$ upon increasing H_2O_2 concentrations (also see in Video S4, ESI†), indicating that PS–Pt colloids that were more chemically active moved with their PS heads more tilted toward the wall. As discussed above, a larger tilt slows down the PS–Pt colloid possibly because the propulsive force is less aligned with its direction of motion. The competition between these two factors – on the one hand, higher chemical activity provides a stronger propulsive force, but on the other hand, it tilts the colloid further toward the wall, so that less of the propulsive force points along the wall – could qualitatively explain why the speeds of PS–Pt colloids saturate at high H_2O_2 concentrations shown in Fig. 3a. A similar saturation of propulsion speed has been reported for chemically powered phoretic active colloids,[43–45] and could potentially be explained by the above competition.

The effect of Pt thickness on the speed and tilt of a 5 μm PS–Pt colloid in 5 v/v% H_2O_2 is examined in Fig. 3c and d. Our measurements show that a PS–Pt colloid coated with a thicker Pt cap moves faster and at a larger θ (its head tilted progressively more toward the wall): a PS colloid coated with 50 nm Pt moved at 6.8 ± 1.4 μm s^{-1} and at a θ of $39.0 \pm 8.7^\circ$, whereas one coated with 5 nm Pt moved at 3.5 ± 0.9 μm s^{-1} and at a θ of $5.9 \pm 2.0^\circ$ (also see Video S5, ESI†). The counterintuitive observation that a PS colloid with a thicker and heavier Pt

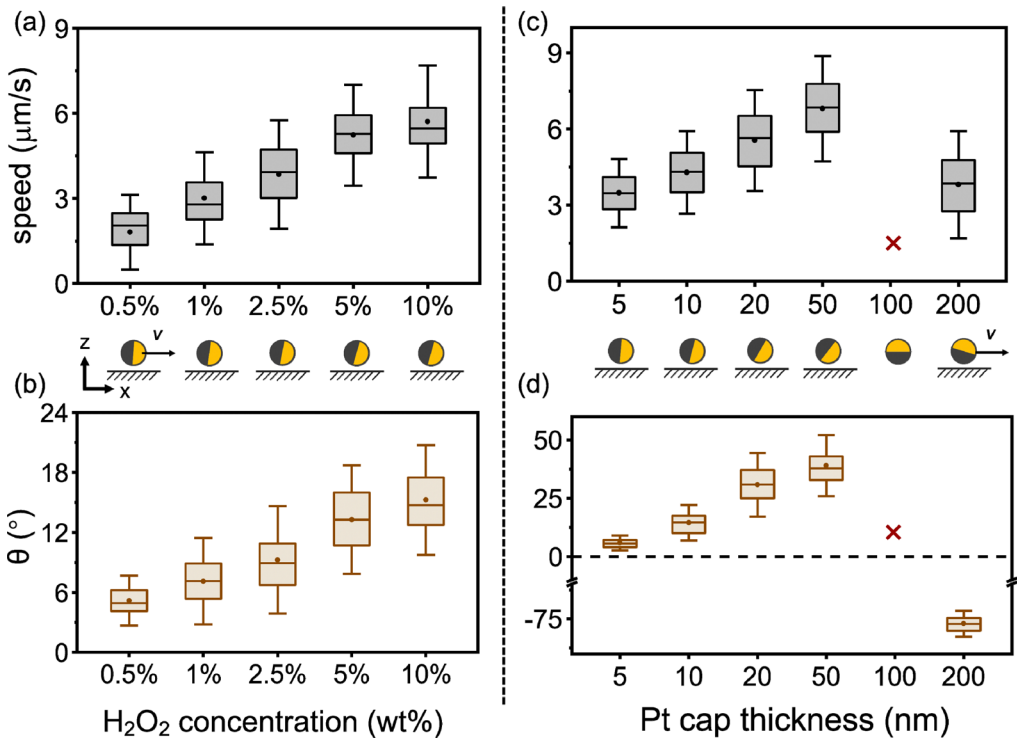

Fig. 3 The self-propulsion speeds and tilt angles (θ) of 5 μm PS–Pt Janus colloids moving along the bottom wall in different H_2O_2 concentrations (a) and (b) and for colloids of different Pt cap thickness (c) and (d). The dot and the horizontal line inside a box plot are the mean and the median, while the top and bottom edge of the box are the first and third quartiles of the data. Side-view cartoons of the corresponding tilting conditions of the Janus colloids are given for illustrative purposes. The red Xs in (c) and (d) for the case of a 100 nm Pt cap are because the colloid does not self-propel along the bottom wall. See the main text for details. Note that the *y* axis in (d) is broken below 0 to accommodate the large negative value for the case of 200 nm Pt cap. Representative data are shown in Videos S4 and S5 (ESI†).

cap moved at a larger θ (*i.e.* heavier metal caps tilted further away from the wall) than one with a thinner Pt coating suggests the competition of two effects. On the one hand, a thicker and thus heavier Pt cap intuitively rotates the PS cap of a PS–Pt colloid away from the bottom wall by gravity (*i.e.*, decreases θ). On the other hand, a thicker Pt is likely more catalytically active for the decomposition of H_2O_2, as an earlier measurement suggests.[46] A more catalytically active Pt cap then possibly increase θ in the same way as increasing the H_2O_2 concentrations. Therefore, the θ at a steady state is determined by the competition of these two contributions—a thicker Pt cap decreases θ because it is heavier but increases θ because it is more catalytically active. The result in Fig. 3c and d could be rationalized by the explanation that the contribution of the Pt coating to the chemical activity dominates that of gravity, but a quantitative, mechanistic understanding is lacking at this moment.

We note two interesting observations in Fig. 3c and d by further increasing the thickness of the Pt coating. First, PS–Pt colloids coated with 100 nm Pt could not stably move along the bottom. Instead, most of them had their Pt caps pointing downwards to the bottom wall (*i.e.* θ close to -90°), and therefore spontaneously moved upward against gravity upon even minor disturbances such as a slight touch on the experimental chamber. Further increasing the Pt coating thickness to 200 nm, however, re-enabled the Janus colloid to move slowly along the bottom wall at 3.8 ± 1.4 μm s^{-1} with its PS side pointing away from the wall at a θ of $-77 \pm 3.7^\circ$. This is possibly because a PS–Pt colloid of 200 nm Pt is too heavy to easily move upward. Currently, we do not fully understand the dynamics of PS–Pt colloids of 100 or 200 nm Pt caps, except to note that earlier studies have suggested the role of surface morphology and the distribution of activity sites on the speeds of Pt Janus active colloids,[47,48] which could become important for thicker Pt caps. The "lift-off" of heavy-bottom PS–Pt colloids, or their unique sliding states with a negative θ along the bottom wall, has been theoretically studied in earlier studies[20] and will be the subject of a future study.

The tilting of the PS–Pt colloids moving in H_2O_2 along the bottom or the top solid wall can be qualitatively understood by a balance between the gravitational torque (T_G) from the heavy Pt cap, and the torque (T_A) arising from the activity of the colloid that tilts it in the opposite direction. A numerical simulation was performed to provide qualitative support to this proposed mechanism. Following ref. 46, our numerical model assumed that PS–Pt moved *via* self-electrophoresis, with the pole and equator of the Pt cap being the cathode and anode of the electrochemical decomposition of H_2O_2 (Fig. 4a), respectively, *i.e.*:

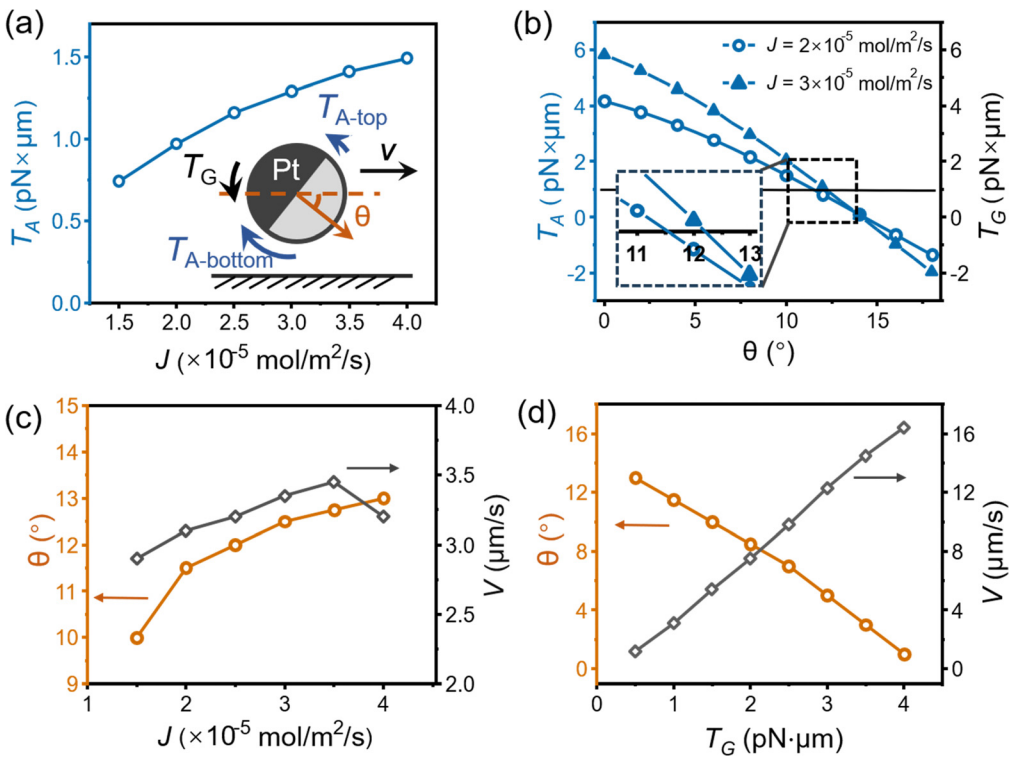

Fig. 4 Understanding the origin of tilts. (a) Calculated activity-induced torque (T_A) of a Pt–PS colloid near the bottom wall at various ionic fluxes (J) on the Pt cap. Inset: Schematic of the gravitational torque (T_G) and the T_A acting on the Janus microsphere. T_A is larger near the bottom because of the strong confinement. See main text for details. (b) Calculated T_A (left) and T_G (right, corresponding to the horizontal solid line) for Janus microspheres fixed at various θ, for two flux values. The steady-state θ is determined for each flux when T_A equals T_G. Inset: Zoomed-in view of the intersections between the results of T_A and T_G. Note how a larger flux leads to a larger θ. See Fig. S13 (ESI†) for more details. (c) and (d) Calculated steady-state θ (left, orange circles) and colloidal speeds V (right, black diamonds) at various fluxes J ((c), corresponding to H_2O_2 concentrations) and T_G ((d), corresponding to the Pt cap thickness).

Cathode (pole):

$$H_2O_2 + 2H^+ + 2e^- \rightarrow 2H_2O$$

Anode (equator):

$$H_2O_2 \rightarrow 2H^+ + O_2 + 2e^-$$

Overall:

$$2H_2O_2 \rightarrow 2H_2O + O_2$$

The proton gradient across the Pt cap establishes a local electric field that points from the equator to the pole, and generates an electroosmotic slip velocity on the negatively charged colloidal surface, which powers the active colloid into autonomous motion away from the Pt cap. We note that although there has been growing experimental evidence for the operation of self-electrophoresis outlined above for a Pt-Janus colloid in H_2O_2,[46] a conclusive proof is not available yet. Nevertheless, this mechanism is assumed in our models.

In addition to leading to directional propulsion, and more pertinent to the current discussion of tilt angles, the electroosmotic slip flows on the surface of the Pt cap also generate a torque (T_A, where A stands for "activity") on the colloid due to the non-slip boundary conditions for the flow. Let us use the case near the bottom wall as an example, while the case near the top wall is qualitatively the same. When viewed from the side and for a PS–Pt that faces the right (Fig. 4a), the electroosmotic torque from below turns it clockwise and the torque from above turns it counter-clockwise. In the absence of a boundary, these torques cancel and $T_A = 0$. However, in the presence of a nearby solid bottom wall, the shear flow and therefore T_A is stronger at the bottom, confined side of the colloid than the top side farther from the wall (see Fig. S13 for more details, ESI†). This asymmetric torque then tilts the colloid moving at the bottom wall into a positive θ. As the Pt cap (especially the equator) tilts away from the wall, however, the electroosmotic flow on the bottom of the colloid becomes less confined and the total T_A smaller, until finally T_A is balanced by T_G at a particular θ (*i.e.*, the steady-state θ).

To calculate T_G, T_A and ultimately the steady-state tilt angle θ where T_A and T_G balances each other, the chemical, electrical and flow fields of a PS–Pt Janus colloid moving above a solid, nonslip, charged surface were simulated using a finite element method (COMSOL version 5.6), by solving for Poisson–Nernst–Planck–Stokes equations in 2D.[16] The Janus sphere was fixed in space and its tilt angle was allowed to vary between different calculations. The T_A acting on the PS–Pt colloid was computed *via* Maxwell σ_E and the hydrodynamic σ_H stress tenors and integrated over the colloidal surface. This calculation of T_A was repeated for multiple θ, until the steady-state θ that generated the T_A that most closely matched T_G (so that $T_A + T_G = 0$) was found. See Fig. 4b for details of this search strategy, where the steady-state θ is where the two lines intersect. Details of our models are given in the ESI,† including governing equations, boundary conditions, parameters used for calculation, meshing, tests for model accuracy, and simulation results of various physical and chemical fields.

Using experimentally relevant parameters (see Table S1, ESI†), our numerical models predicted θ values of a few degrees for 5 μm PS–Pt colloids moving in H_2O_2 along the bottom wall (Fig. 4c and d), in qualitative agreement with the experimental values reported above. Moreover, our models predicted that PS–Pt active colloids would tilt further toward the wall at higher surface ionic fluxes (*i.e.*, in more concentrated H_2O_2 solutions, see Fig. 4c), consistent with the experimental observations in Fig. 3a. A qualitative explanation is that, as the flux (H_2O_2 concentration) increases, so does the magnitude of the surface electroosmotic flow, which consequently increases T_A. As a result, the increased T_A now balance T_G at a new, larger θ (see Fig. 4b for a detailed example of how increased fluxes lead to a larger steady-state θ).

Our models made the interesting, counterintuitive predictions that the colloidal speeds peaked at an intermediate chemical flux of $\sim 3 \times 10^{-5}$ mol m^{-2} s^{-1}. This peak in speeds could be due to a competition of two effects from increasing the flux. On the one hand it provides more propulsion force so that the speed increases. One the other hand, it pulls the colloid closer to the bottom wall[16] and increases the activity-induced torque (T_A) so that θ increases, both decreasing the propulsion speed. Such a competition could explain the scattered report in the literature of similar counterintuitive decrease in propulsion speeds of chemically powered active colloids at high fuel concentrations.[44,49] Even though the PS–Pt colloids in our experiments did not move more slowly at higher concentrations of H_2O_2, the rate of increase in speeds indeed slowed at H_2O_2 concentrations up to 10% (Fig. 3a). Moreover, we indeed occasionally observe that they moved more slowly at higher H_2O_2 concentrations, but such observations were poorly reproducible.

Our models also predicted that the tilt angle would monotonically decrease for Pt-Janus colloids with larger gravitational torques (*i.e.*, heavier Pt caps, see Fig. 4d). A qualitative explanation is that, increasing the Pt cap while assuming constant surface flux raises the T_G values (effectively raising the black line in Fig. 4b), so that T_A and T_G are now balanced at a smaller θ. This prediction of smaller θ for heavier Pt caps was, however, contrary to our experimental observations in Fig. 3d that showed higher θ for thicker Pt caps. This discrepancy can be attributed to the model's assumption that the surface flux was the same for metal caps of different thicknesses, yet, as we suggested earlier, the surface chemical flux likely varies in reality and potentially even nonlinearly over Pt thickness. In addition, the coverage of the Pt cap could change at different cap thickness. For example, Fig. S14 (ESI†) shows preliminary simulation results that increasing the chemical flux and the area of the Pt coverage could lead to larger, instead of smaller, θ values for a thicker Pt cap. However, the lack of the exact information of how the flux or the Pt coverage varies over Pt thickness prevented us from making solid conclusions.

Discussion and conclusions

Taking advantage of fluorescent microspheres and AC electric fields, we measured the tilt angle – defined as the angle

between the wall and the line connecting the two caps of the colloid – of PS–Pt and SiO_2–Pt Janus colloids moving in H_2O_2 along a solid wall. Typical values of the tilt angle were 13.3° or −33.9° for 5 μm PS microspheres half-coated with 10 nm Pt moving in 5% H_2O_2 along a bottom or top glass wall, respectively, indicating that these colloids moved with their PS caps tilted toward the wall. For PS–Pt colloids moving in the bulk, near the top and the bottom wall, we found that $|\langle\theta_{bulk}\rangle| > |\langle\theta_{top}\rangle| > |\langle\theta_{bottom}\rangle|$, and $\langle V_{bulk}\rangle > \langle V_{bottom}\rangle > \langle V_{top}\rangle$ for the tilt angles and the self-propulsion speeds, respectively. The tilt angles and propulsion speeds of PS–Pt colloids at the bottom wall increased with higher concentrations of H_2O_2 and, less intuitively, with thicker Pt caps. A finite element simulation based on self-electrophoresis offers a possible explanation for the tilt: it results from a balance between the torque due to gravity and the combined torque due to electrostatics and hydrodynamics that arise from the self-generated chemical gradients. Notably, our 2D model is based on colloidal electrokinetics and calculated the torques by solving for the full electrical double layers, which distinguishes it from earlier studies that have examined the tilt angles of similar active colloids and even proposed theoretical explanations (see below).

Although only one type of active colloids is studied here (*i.e.* those half-coated with Pt and moving in H_2O_2), we speculate that other types of chemically powered, autophoretic colloids could also move along a boundary with a non-zero tilt, such as those half-coated with Ag,[50] PtO,[51] TiO_2,[52] or those containing two chemically active caps such as Au–Pt microrods[44] and microspheres[45] in H_2O_2, or TiO_2–Pt Janus microspheres under UV light.[16] However, whether they move with a tilt or how large the tilt is could depend sensitively on the distributions of chemical activity on the colloidal surface, the magnitude of the surface chemical fluxes, and particle properties such as shapes,[53,54] sizes, surface chemistry,[55] and surface roughness.[46,56] Moreover, the material properties of the wall, such as its wettability, surface charges, or roughness, could also significantly affect the tilt angles of nearby active colloids, in a similar way to how they affect the colloidal speeds.[15,57] This is a likely source of the mixed reports of zero and non-zero tilts in the literature.

From the experimental point view, this uncertainty can be clarified by measuring the tilt angle of a fluorescent particle, possibly aided by an AC electric field or magnetic fields, as we did in the current study or in ref. 42. However, we do note that the acquisition of fluorescent micrographs of high quality and sharp contrast, and a reference image based on which the moon phase is calculated, is critical to extracting correct tilt angles, yet non-trivial and prone to errors. An additional experimental challenge is that many types of active colloids cannot be made from fluorescent polymer or SiO_2 beads, and therefore require a different technique to measure their tilt angles.

Our numerical models for explaining the tilts are limited in the following aspects. First, due to computational costs, particularly an extremely fine meshing at the boundary layer, our numerical models are in 2D, and we expect a 3D model to be different in the distribution of chemical concentrations, the structure of the electrical double layers, and the details of the hydrodynamics. These differences could lead to a smaller hydrodynamic torque in a 3D model where part of the sphere is farther from the wall than a 2D model. Second, our current model requires a Pt coverage of >50% on the colloidal surface for it to slide stably on both the top and the bottom wall. Our experimental observations, however, were not bound by this requirement. Third, our model assumes the active colloid is powered by self-electrophoresis and that the equator and the pole of the Pt cap is the anode and the cathode, respectively. These assumptions are based on previously studies and reasonable,[46,51,58,59] but have not been experimentally confirmed. Finally, the predicted values of θ, and how it changes over chemical fluxes or cap weight, does not quantitatively match experimental results. One possible source of these discrepancies could be the high sensitivity of the simulation result to the height of the colloid, which was challenging to determine accurately. The other source could be the assumption of constant chemical flux and Pt coverage for Pt caps of different thickness. Despite these limitations, the order-of-magnitude agreement between the predicted and measured θ values qualitatively suggests that the PS–Pt active colloid's tilting behavior near a solid wall can be explained by self-electrophoresis and its electrostatic and hydrodynamic interactions with the boundary.

Two earlier studies of the orientation of chemically powered active colloids near a solid wall are worth comparing with the current study. First, a model similar to ours was proposed in ref. 22 to explain the tilt of a chemically active, Janus colloids moving near solid walls. It assumed neutral self-diffusiophoresis for the active colloids, and solved for the torques from chemical activity, hydrodynamics, and gravity, which combine to determine the steady state θ. This study also predicted that an active colloid that release solutes from one side, such as PS–Pt, could stably slide along both the top and bottom walls, with their unreactive caps tilted toward the wall. These conclusions are qualitatively consistent with our experimental data and our numerical simulations. The key difference is the propulsion mechanism, and therefore the forces contributing to motion and torques, in our models (self-electrophoresis) and that in ref. 22 (neutral s-diffusiophoresis). However, we emphasize that the current study is not intended to challenge the results in ref. 22, but rather to provide an alternative perspective centered around electrokinetic effects. In fact, it is possible these two mechanisms coexist in our experiments and both generate torques, one from the gradients of neutral molecule such as H_2O_2 and O_2, and the other from the self-generated electric fields.

The second study worth discussing is ref. 11, which experimentally observed, and theoretically explained, that the same PS–Pt Janus microsphere as we experimented with would move in H_2O_2 along a solid wall with a zero tilt (or a polar angle of 90° in their definition), so that its Janus interface is perfectly perpendicular to the wall. This was especially clear in ref. 11 for spheres of 1.55 or 2.4 μm in diameter, while the smaller sphere of 1 μm in diameter moved with its unreactive cap slightly tilted toward the wall. These values of tilt angle were obtained from the moon phases of florescent microspheres

similar to ours. In order to explain such a zero tilt, the authors of ref. 11 simulated the electrostatics and hydrodynamics of a PS–Pt colloid near a solid wall, assuming self-electrophoresis, and were able to find a set of parameters that led to zero tilt. The experimental and theoretical values of the tilt angles reported in ref. 11 are different from the current study possibly for the following reasons. First, the "halos" in the optical micrographs in Fig. 1a of ref. 11 could lead to small errors in the measurement of the fluorescence intensity of half-moons, and consequently lead to errors in the determination of θ, especially for small θ. Such errors were mitigated in our study through the use of reference images obtained under AC electric fields. Second, the thin Pt coating (10 nm) used in ref. 11 could also lead to a small θ (as suggested in Fig. 3d here) that further contributes to the errors. Third, the electrostatic torque is calculated differently between ref. 11 and our work. In ref. 11, this is assumed to arise from an alignment of the particle's zeta potential dipole with its self-generated electric field, while we simulated the complete electrical double layer and calculated the stress tensor.

It is also interesting to note that SiO_2–Au Janus microspheres were found to move with a tilt along an optical fiber,[60] powered by optical forces from evanescent waves. There, the tilt was a result of the torque balance between gravity, friction and optical forces. However, we do not discuss any further because of the apparent difference between these optically powered Janus colloids and ours that are chemically powered.

To summarize, by experimentally measuring the tilt, proposing a likely origin, and showing how the tilt changes under different experimental conditions, this study sheds important light on understanding how chemically active colloids move and interact with solid boundaries. This study builds on and extends the findings of two earlier studies on the orientations of passive Janus particles near walls[61] by showing that for an active Janus colloid, cap weight alone does not fully dictate orientation—rather, the competition between gravitational torque and activity-induced torque determines the final tilt. Furthermore, although we have focused on PS–Pt active colloids, it is reasonable to speculate that other active colloids driven by self-generated chemical gradients also move along a wall with a tilt. We therefore caution the active colloid community against assuming that a self-propelled active colloid moves with a zero tilt along a boundary. They could very well still do so, but not necessarily. We also draw the community's attention to the possible effects of such tilts on the speeds, directionality, and interaction of a chemically active colloid with a boundary.

Data availability

The data that supports the findings of this study are available in the ESI† of this article.

Conflicts of interest

There are no conflicts to declare.

Acknowledgements

Wei Wang and Xing Ma are funded by National Key R&D Program of China (2023YFE0208700) Jiayu Liu, Zihan Qiao, Ting Kuang and Wei Wang are financially supported by the National Natural Science Foundation of China (T2322006) and the Shenzhen Science and Technology Program (RCYX20210609103122038 and JCYJ20210324121408022). Shanshan Li and Xing Ma are supported by the Shenzhen Science and Technology Program (RCJC20231211090000001 and GXWD20231129101105001). Yankai Xu and H. P. Zhang acknowledge financial support of the NSFC (No. 12225410 and No. 12074243) and the Student Innovation Center at Shanghai Jiao Tong University. Wei Wang and H. P. Zhang are financially supported by the China Manned Space Engineering Program (Project number: KJZ-YY-NLT0502).

References

1 W. Chen, Y. Song, Y. Liu, J. Chen and X. Ma, Chemically Powered Active Colloids. in *Active Colloids: From Fundamentals to Frontiers*, ed. W. Wang, J. Simmchen, W. Uspal, Royal Society of Chemistry, 2024, vol. 20.
2 W. Wang, Open Questions of Chemically Powered Nano- and Micromotors, *J. Am. Chem. Soc.*, 2023, **145**(50), 27185–27197, DOI: **10.1021/jacs.3c09223**.
3 J. T. Ault and S. Shin, Physicochemical Hydrodynamics of Particle Diffusiophoresis Driven by Chemical Gradients, *Annu. Rev. Fluid Mech.*, 2025, **57**, 227–255, DOI: **10.1146/annurev-fluid-030424-110950**.
4 B. Jang, M. Ye, A. Hong, X. Wang, X. Liu, D. Bae, J. Puigmartí Luis and S. Pané, Catalytically Propelled Micro- and Nanoswimmers, *Small Sci.*, 2023, **3**(11), 2300076, DOI: **10.1002/smsc.202300076**.
5 M. J. Bowick, N. Fakhri, M. C. Marchetti and S. Ramaswamy, Symmetry, Thermodynamics, and Topology in Active Matter, *Phys. Rev. X*, 2022, **12**(1), 010501, DOI: **10.1103/PhysRevX.12.010501**.
6 K. J. M. Bishop, S. L. Biswal and B. Bharti, Active Colloids as Models, Materials, and Machines, *Annu. Rev. Chem. Biomol. Eng.*, 2023, **14**, 1–30, DOI: **10.1146/annurev-chembioeng-101121-084939**.
7 W. Wang, X. Lv, J. L. Moran, S. Duan and C. Zhou, A practical guide to active colloids: choosing synthetic model systems for soft matter physics research, *Soft Matter*, 2020, **16**(16), 3846–3868, DOI: **10.1039/D0SM00222D**.
8 A. Al Harraq, M. Bello and B. Bharti, A guide to design the trajectory of active particles: From fundamentals to applications, *Curr. Opin. Colloid Interface Sci.*, 2022, **61**, 101612, DOI: **10.1016/j.cocis.2022.101612**.
9 J. Li and J. Yu, Biodegradable Microrobots and Their Biomedical Applications: A Review, *Nanomaterials*, 2023, **13**(10), 1590.
10 Y. Fu, H. Yu, X. Zhang, P. Malgaretti, V. Kishore and W. Wang, Microscopic Swarms: From Active Matter Physics to Biomedical and Environmental Applications, *Micromachines*, 2022, **13**(2), 295.

11 S. Das, A. Garg, A. I. Campbell, J. Howse, A. Sen, D. Velegol, R. Golestanian and S. J. Ebbens, Boundaries can steer active Janus spheres, *Nat. Commun.*, 2015, **6**(1), 8999, DOI: 10.1038/ncomms9999.
12 J. Simmchen, J. Katuri, W. E. Uspal, M. N. Popescu, M. Tasinkevych and S. Sánchez, Topographical pathways guide chemical microswimmers, *Nat. Commun.*, 2016, **7**(1), 10598, DOI: 10.1038/ncomms10598.
13 C. Liu, C. Zhou, W. Wang and H. P. Zhang, Bimetallic Microswimmers Speed Up in Confining Channels, *Phys. Rev. Lett.*, 2016, **117**(19), 198001, DOI: 10.1103/PhysRevLett.117.198001.
14 T.-Y. Chiang and D. Velegol, Localized Electroosmosis (LEO) Induced by Spherical Colloidal Motors, *Langmuir*, 2014, **30**(10), 2600–2607, DOI: 10.1021/la402262z.
15 S. Ketzetzi, J. de Graaf, R. P. Doherty and D. J. Kraft, Slip Length Dependent Propulsion Speed of Catalytic Colloidal Swimmers near Walls, *Phys. Rev. Lett.*, 2020, **124**(4), 048002, DOI: 10.1103/PhysRevLett.124.048002.
16 Y. Xu, C. Liu, J. Liu, P. Xu, Z. Xiao, W. Wang and H. P. Zhang, Measuring Attractive Interaction between a Self-Electrophoretic Micromotor and a Wall, *Phys. Rev. Lett.*, 2024, **133**(25), 258304, DOI: 10.1103/PhysRevLett.133.258304.
17 Z. Xiao, S. Duan, P. Xu, J. Cui, H. Zhang and W. Wang, Synergistic Speed Enhancement of an Electric-Photochemical Hybrid Micromotor by Tilt Rectification, *ACS Nano*, 2020, **14**(7), 8658–8667, DOI: 10.1021/acsnano.0c03022.
18 A. T. Brown, I. D. Vladescu, A. Dawson, T. Vissers, J. Schwarz-Linek, J. S. Lintuvuori and W. C. K. Poon, Swimming in a crystal, *Soft Matter*, 2016, **12**(1), 131–140, DOI: 10.1039/C5SM01831E.
19 S. Ketzetzi, J. de Graaf and D. J. Kraft, Diffusion-Based Height Analysis Reveals Robust Microswimmer-Wall Separation, *Phys. Rev. Lett.*, 2020, **125**(23), 238001, DOI: 10.1103/PhysRevLett.125.238001.
20 A. Mozaffari, N. Sharifi-Mood, J. Koplik and C. Maldarelli, Self-diffusiophoretic colloidal propulsion near a solid boundary, *Phys. Fluids*, 2016, **28**(5), 053107, DOI: 10.1063/1.4948398 (acccessed 12/31/2024).
21 W. E. Uspal, M. N. Popescu, S. Dietrich and M. Tasinkevych, Self-propulsion of a catalytically active particle near a planar wall: from reflection to sliding and hovering, *Soft Matter*, 2015, **11**(3), 434–438, DOI: 10.1039/C4SM02317J.
22 S. Das, Z. Jalilvand, M. N. Popescu, W. E. Uspal, S. Dietrich and I. Kretzschmar, Floor- or Ceiling-Sliding for Chemically Active, Gyrotactic, Sedimenting Janus Particles, *Langmuir*, 2020, **36**(25), 7133–7147, DOI: 10.1021/acs.langmuir.9b03696.
23 V. Carrasco-Fadanelli and I. Buttinoni, Sedimentation and levitation of catalytic active colloids, *Phys. Rev. Res.*, 2023, **5**(1), L012018, DOI: 10.1103/PhysRevResearch.5.L012018.
24 T. Li, A. Zhang, G. Shao, M. Wei, B. Guo, G. Zhang, L. Li and W. Wang, Janus Microdimer Surface Walkers Propelled by Oscillating Magnetic Fields, *Adv. Funct. Mater.*, 2018, **28**(25), 1706066, DOI: 10.1002/adfm.201706066.
25 R. Barnkob and M. Rossi, General defocusing particle tracking: fundamentals and uncertainty assessment, *Exp. Fluids*, 2020, **61**(4), 110, DOI: 10.1007/s00348-020-2937-5.
26 S. M. Anthony, L. Hong, M. Kim and S. Granick, Single-Particle Colloid Tracking in Four Dimensions, *Langmuir*, 2006, **22**(24), 9812–9815, DOI: 10.1021/la062094h.
27 S. Gangwal, O. J. Cayre, M. Z. Bazant and O. D. Velev, Induced-Charge Electrophoresis of Metallodielectric Particles, *Phys. Rev. Lett.*, 2008, **100**(5), 058302, DOI: 10.1103/PhysRevLett.100.058302.
28 J. L. Moran and J. D. Posner, Electrokinetic locomotion due to reaction-induced charge auto-electrophoresis, *J. Fluid Mech.*, 2011, **680**, 31–66, DOI: 10.1017/jfm.2011.132 From Cambridge University Press Cambridge Core.
29 J. L. Moran and J. D. Posner, Role of solution conductivity in reaction induced charge auto-electrophoresis, *Phys. Fluids*, 2014, **26**(4), 042001, DOI: 10.1063/1.4869328 (acccessed 1/16/2025).
30 A. T. Brown, W. C. K. Poon, C. Holm and J. de Graaf, Ionic screening and dissociation are crucial for understanding chemical self-propulsion in polar solvents, *Soft Matter*, 2017, **13**(6), 1200–1222, DOI: 10.1039/C6SM01867J.
31 J. L. Moran and J. D. Posner, Phoretic Self-Propulsion, *Annu. Rev. Fluid Mech.*, 2017, **49**, 511–540, DOI: 10.1146/annurev-fluid-122414-034456.
32 A. M. Brooks, M. Tasinkevych, S. Sabrina, D. Velegol, A. Sen and K. J. M. Bishop, Shape-directed rotation of homogeneous micromotors *via* catalytic self-electrophoresis, *Nat. Commun.*, 2019, **10**(1), 495, DOI: 10.1038/s41467-019-08423-7.
33 M. De Corato, X. Arqué, T. Patiño, M. Arroyo, S. Sánchez and I. Pagonabarraga, Self-Propulsion of Active Colloids via Ion Release: Theory and Experiments, *Phys. Rev. Lett.*, 2020, **124**(10), 108001, DOI: 10.1103/PhysRevLett.124.108001.
34 T. V. Nizkaya, E. S. Asmolov and O. I. Vinogradova, Theoretical modeling of catalytic self-propulsion, *Curr. Opin. Colloid Interface Sci.*, 2022, **62**, 101637, DOI: 10.1016/j.cocis.2022.101637.
35 A. Shrestha and M. Olvera de la Cruz, Enhanced phoretic self-propulsion of active colloids through surface charge asymmetry, *Phys. Rev. E*, 2024, **109**(1), 014613, DOI: 10.1103/PhysRevE.109.014613.
36 J. Liu, Z. Yang, Z. Yan, S. Duan, X. Chen, D. Cui, D. Cao, T. Kuang, X. Ma and W. Wang, Chemical Micromotors Move Faster at Oil–Water Interfaces, *J. Am. Chem. Soc.*, 2024, **146**(6), 4221–4233, DOI: 10.1021/jacs.3c13743.
37 W. E. Uspal, M. N. Popescu, S. Dietrich and M. Tasinkevych, Rheotaxis of spherical active particles near a planar wall, *Soft Matter*, 2015, **11**(33), 6613–6632, DOI: 10.1039/C5SM01088H.
38 J. N. Anker and R. Kopelman, Magnetically modulated optical nanoprobes, *Appl. Phys. Lett.*, 2003, **82**(7), 1102–1104, DOI: 10.1063/1.1544435 (acccessed 12/31/2024).
39 C. J. Behrend, J. N. Anker, B. H. McNaughton, M. Brasuel, M. A. Philbert and R. Kopelman, Metal-Capped Brownian and Magnetically Modulated Optical Nanoprobes (MOONs): Micromechanics in Chemical and Biological Microenvironments, *J. Phys. Chem. B*, 2004, **108**(29), 10408–10414, DOI: 10.1021/jp040125g.
40 S. J. Ebbens and J. R. Howse, Direct Observation of the Direction of Motion for Spherical Catalytic Swimmers,

Langmuir, 2011, **27**(20), 12293–12296, DOI: **10.1021/la2033127**.

41 S. A. Nabavizadeh, J. Castañeda, J. G. Gibbs and A. Nourhani, Gravitropically Stabilized Self-Assembly of Active Microcrystallites and Spinning Free Janus Particles, *Part. Part. Syst. Charact.*, 2022, **39**(1), 2100232, DOI: **10.1002/ppsc.202100232**.

42 A. Boymelgreen, G. Kunti, P. García-Sánchez and G. Yossifon, The influence of frequency and gravity on the orientation of active metallo-dielectric Janus particles translating under a uniform applied alternating-current electric field, *Soft Matter*, 2024, **20**(20), 4143–4151, DOI: **10.1039/D3SM01640D**.

43 M. Manjare, Y. Ting Wu, B. Yang and Y.-P. Zhao, Hydrophobic catalytic Janus motors: Slip boundary condition and enhanced catalytic reaction rate, *Appl. Phys. Lett.*, 2014, **104**(5), 054102, DOI: **10.1063/1.4863952** (acccessed 12/31/2024).

44 W. F. Paxton, K. C. Kistler, C. C. Olmeda, A. Sen, S. K. St. Angelo, Y. Cao, T. E. Mallouk, P. E. Lammert and V. H. Crespi, Catalytic Nanomotors: Autonomous Movement of Striped Nanorods, *J. Am. Chem. Soc.*, 2004, **126**(41), 13424–13431, DOI: **10.1021/ja047697z**.

45 T.-C. Lee, M. Alarcón-Correa, C. Miksch, K. Hahn, J. G. Gibbs and P. Fischer, Self-Propelling Nanomotors in the Presence of Strong Brownian Forces, *Nano Lett.*, 2014, **14**(5), 2407–2412, DOI: **10.1021/nl500068n**.

46 X. Lyu, X. Liu, C. Zhou, S. Duan, P. Xu, J. Dai, X. Chen, Y. Peng, D. Cui and J. Tang, *et al.*, Active, Yet Little Mobility: Asymmetric Decomposition of H2O2 Is Not Sufficient in Propelling Catalytic Micromotors, *J. Am. Chem. Soc.*, 2021, **143**(31), 12154–12164, DOI: **10.1021/jacs.1c04501**.

47 L. Lei, R. Cheng, Y. Zhou, T. Yang, B. Liang, S. Wang, X. Zhang, G. Lin and X. Zhou, Estimating the velocity of chemically-driven Janus colloids considering the anisotropic concentration field, *Front. Chem.*, 2022, **10**, 973961, DOI: **10.3389/fchem.2022.973961**, original research.

48 Z. H. Shah, S. Wang, L. Xian, X. Zhou, Y. Chen, G. Lin and Y. Gao, Highly efficient chemically-driven micromotors with controlled snowman-like morphology, *Chem. Commun.*, 2020, **56**(97), 15301–15304, DOI: **10.1039/D0CC06812H**.

49 R. Laocharoensuk, J. Burdick and J. Wang, Carbon-Nanotube-Induced Acceleration of Catalytic Nanomotors, *ACS Nano*, 2008, **2**(5), 1069–1075, DOI: **10.1021/nn800154g**.

50 X. Liu, Y. Peng, Z. Yan, D. Cao, S. Duan and W. Wang, Oscillations of the Local pH Reverses Silver Micromotors in H2O2, *ChemSystemsChem*, 2024, **6**(6), e202400046, DOI: **10.1002/syst.202400046**.

51 X. Lyu, J. Chen, J. Liu, Y. Peng, S. Duan, X. Ma and W. Wang, Reversing a Platinum Micromotor by Introducing Platinum Oxide, *Angew. Chem., Int. Ed.*, 2022, **61**(24), e202201018, DOI: **10.1002/anie.202201018**.

52 C. Chen, F. Mou, L. Xu, S. Wang, J. Guan, Z. Feng, Q. Wang, L. Kong, W. Li and J. Wang, *et al.*, Light-Steered Isotropic Semiconductor Micromotors, *Adv. Mater.*, 2017, **29**(3), 1603374, DOI: **10.1002/adma.201603374**.

53 J. G. Gibbs, Shape- and Material-Dependent Self-Propulsion of Photocatalytic Active Colloids, Interfacial Effects, and Dynamic Interparticle Interactions, *Langmuir*, 2020, **36**(25), 6938–6947, DOI: **10.1021/acs.langmuir.9b02866**.

54 Z. Wang, Y. Mu, D. Lyu, M. Wu, J. Li, Z. Wang and Y. Wang, Engineering shapes of active colloids for tunable dynamics, *Curr. Opin. Colloid Interface Sci.*, 2022, **61**, 101608, DOI: **10.1016/j.cocis.2022.101608**.

55 Z. Xiao, J. Chen, S. Duan, X. Lv, J. Wang, X. Ma, J. Tang and W. Wang, Bimetallic coatings synergistically enhance the speeds of photocatalytic TiO_2 micromotors, *Chem. Commun.*, 2020, **56**(34), 4728–4731, DOI: **10.1039/D0CC00212G**.

56 U. Choudhury, L. Soler, J. G. Gibbs, S. Sanchez and P. Fischer, Surface roughness-induced speed increase for active Janus micromotors, *Chem. Commun.*, 2015, **51**(41), 8660–8663, DOI: **10.1039/C5CC01607J**.

57 M. Wei, C. Zhou, J. Tang and W. Wang, Catalytic Micromotors Moving Near Polyelectrolyte-Modified Substrates: The Roles of Surface Charges, Morphology, and Released Ions, *ACS Appl. Mater. Interfaces*, 2018, **10**(3), 2249–2252, DOI: **10.1021/acsami.7b18399**.

58 A. Brown and W. Poon, Ionic effects in self-propelled Pt-coated Janus swimmers, *Soft Matter*, 2014, **10**(22), 4016–4027, DOI: **10.1039/C4SM00340C**.

59 S. Ebbens, D. A. Gregory, G. Dunderdale, J. R. Howse, Y. Ibrahim, T. B. Liverpool and R. Golestanian, Electrokinetic effects in catalytic platinum-insulator Janus swimmers, *Europhys. Lett.*, 2014, **106**(5), 58003, DOI: **10.1209/0295-5075/106/58003**.

60 G. Tkachenko, V. G. Truong, C. L. Esporlas, I. Sanskriti and S. Nic Chormaic, Evanescent field trapping and propulsion of Janus particles along optical nanofibers, *Nat. Commun.*, 2023, **14**(1), 1691, DOI: **10.1038/s41467-023-37448-2**.

61 A. Rashidi and C. L. Wirth, Motion of a Janus particle very near a wall, *J. Chem. Phys.*, 2017, **147**(22), 224906, DOI: **10.1063/1.4994843** (acccessed 3/12/2025).

Quantifying and Understanding the Tilt of a Pt Janus Active Colloid Near Solid Walls

Jiayu Liu[1#], Yankai Xu[2#], Zihan Qiao[1], Shanshan Li[3], Xing Ma[3, 4], Ting Kuang[5], H. P. Zhang[2]*, Wei Wang[1]*

1 School of Materials Science and Engineering, Harbin Institute of Technology (Shenzhen), Shenzhen, China, 518055

2 School of Physics and Astronomy, Institute of Natural Sciences and MOE-LSC,

Shanghai Jiao Tong University, Shanghai 200240, China

3 School of Integrated Circuits, Harbin Institute of Technology (Shenzhen), Shenzhen 518055, China

4 Sauvage Laboratory for Smart Materials, School of Materials Science and Engineering, Harbin Institute of Technology (Shenzhen), Shenzhen 518055, China

5 Education Center of Experiments and Innovations, Harbin Institute of Technology (Shenzhen), Shenzhen, China, 518055

Contact author: weiwangsz@hit.edu.cn

Contact author: hepeng_zhang@sjtu.edu.cn

#: authors contributed equally

I. EXPERIMENTS

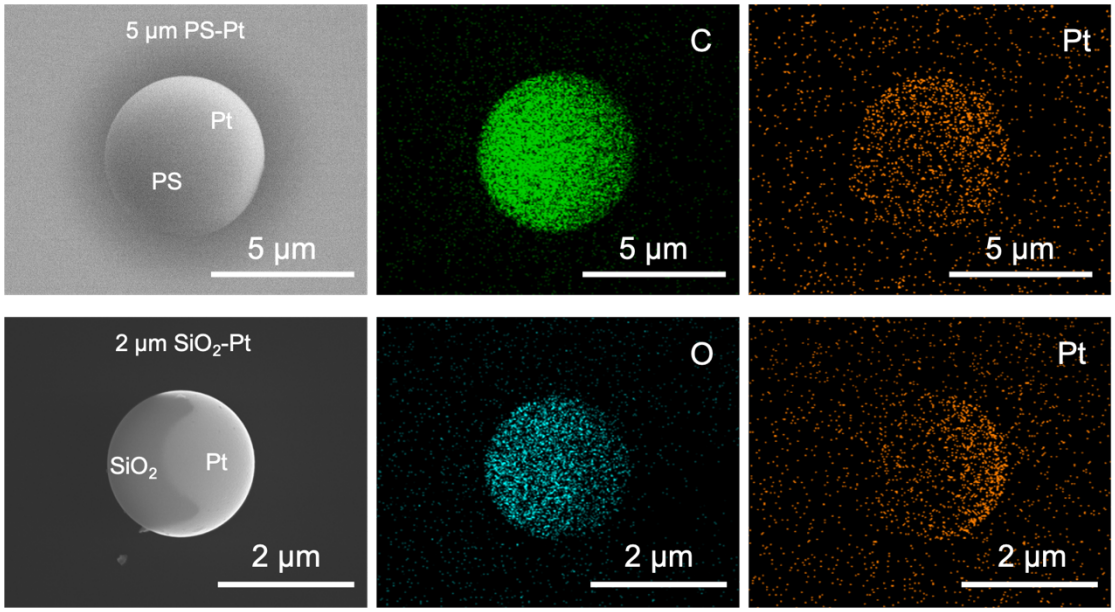

Figure S1. SEM and EDS mapping of 5 μm PS-Pt and 2 μm SiO_2-Pt Janus microspheres.

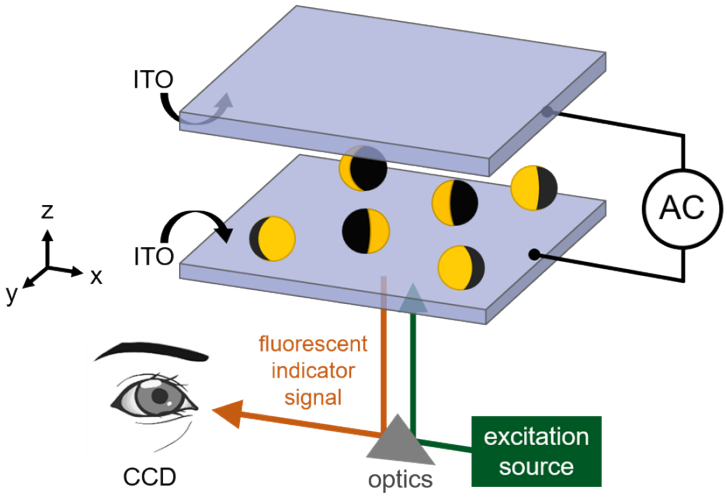

Figure S2. Schematic diagram of the experimental chamber with Janus Pt colloids sandwiched between two pieces of ITOs.

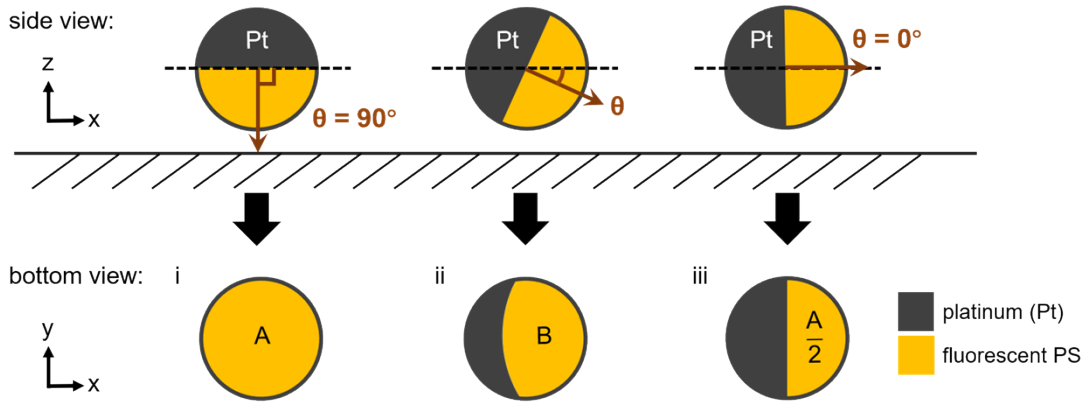

Figure S3. Schematic illustration of the moon phases and corresponding tilt angles of Janus Pt colloids: i) side and bottom view of a Janus motor with tilt angle θ = 90°, ii) side and bottom view of a Janus motor with a non-zero θ, iii) side and bottom view of a Janus motor with θ = 0°, which is experimentally realized by the application of a vertical electric field.

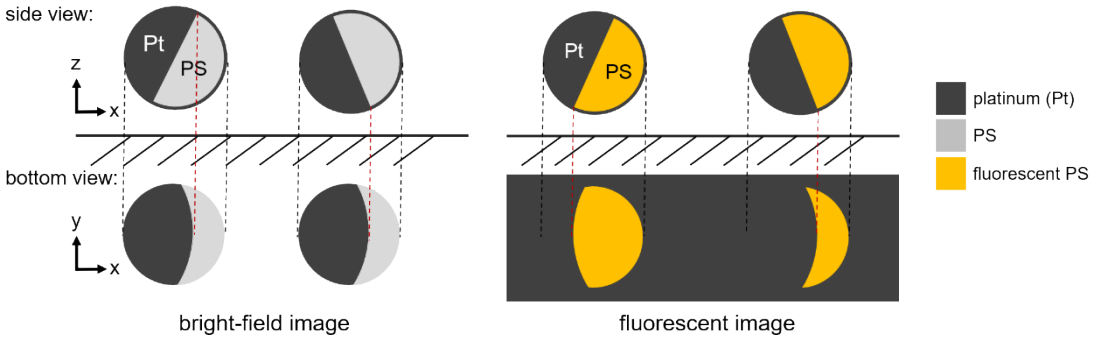

Figure S4. Schematic illustration of the differences of the moon phases of Janus Pt colloids acquired by bright-field microscopy (left) and epi fluorescence microscopy (right). Note how bright field images cannot distinguish between the two configurations.

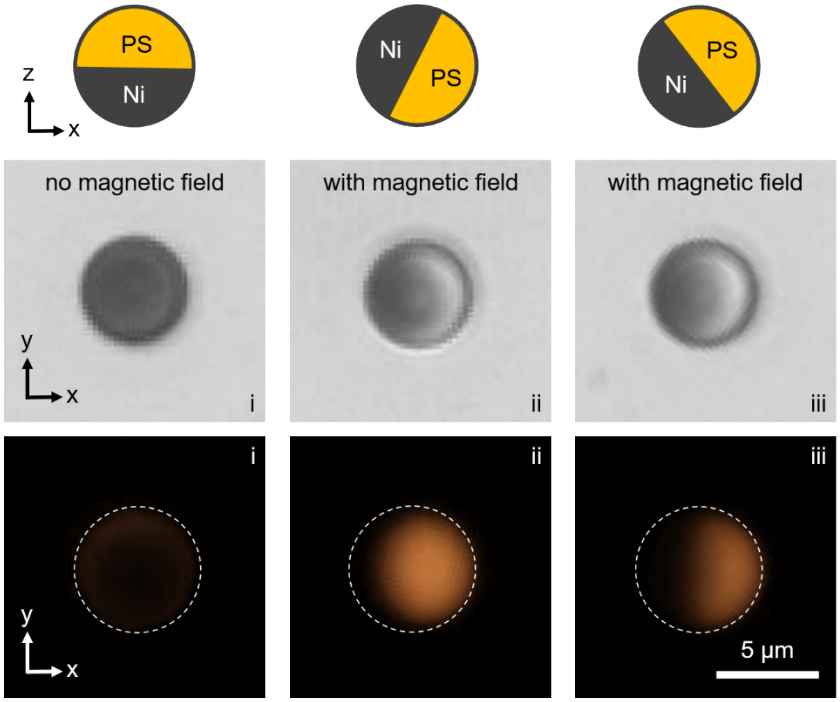

Figure S5. The differences in the optical micrographs of 5 μm Janus PS-Ni colloids acquired by bright-field microscopy (center row) and epi fluorescent microscopy (bottom row). A handheld magnet was used to tilt the Janus sphere.

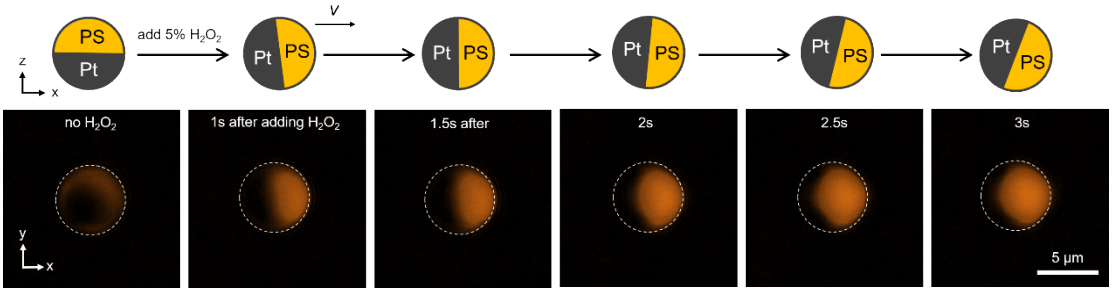

Figure S6. A 5 μm PS-Pt colloid gradually flipped and started to move after the addition of 5% H_2O_2, with 10 nm Pt cap.

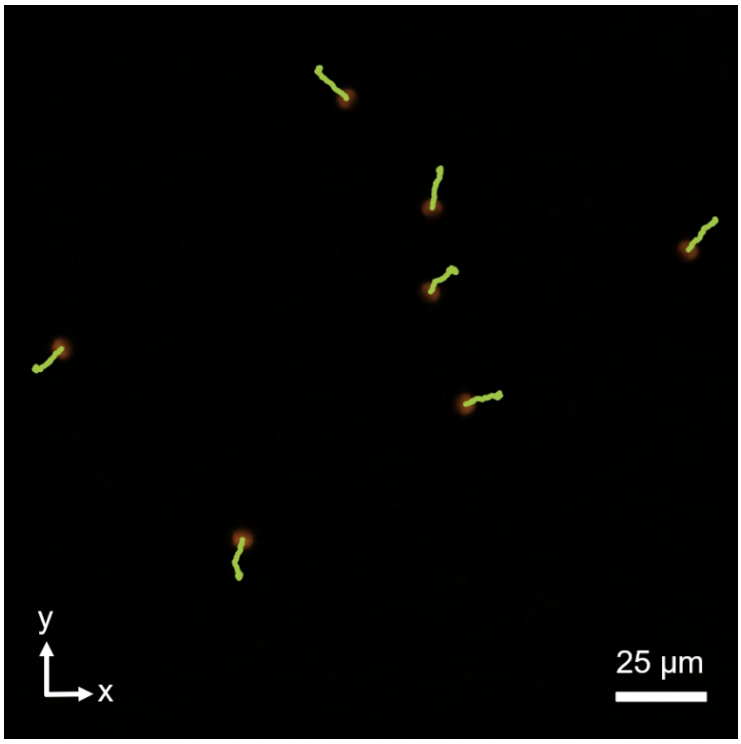

Figure S7. 10 s trajectory of 5 μm Janus PS-Pt colloids in 5% H_2O_2, under a sinusoidal AC electric field of 1 MHz and a time averaged electric field strength of 17.7 V/mm .

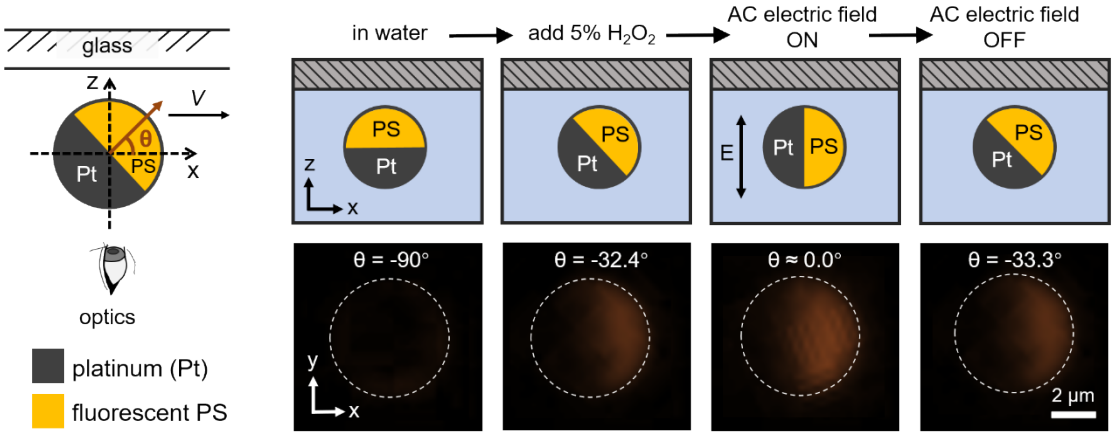

Figure S8. Quantifying the θ of a 5 μm PS-Pt Janus active colloid moving along a top ceiling in 5% H_2O_2. The colloid was coated with 10 nm Pt cap.

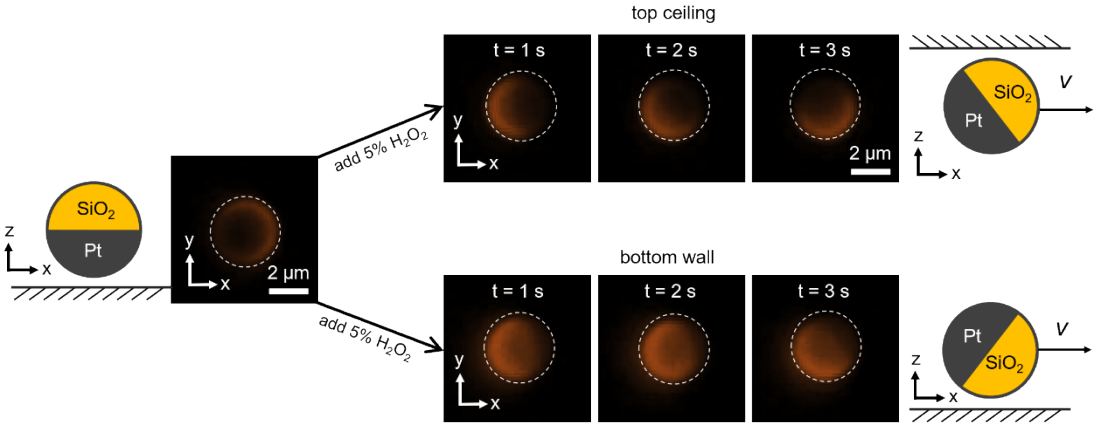

Figure S9. Fluorescence imaging of SiO_2-Pt Janus colloids moving in 5% H_2O_2 along the bottom wall and top ceiling. The colloid was coated with 10 nm Pt cap.

II. NUMERICAL METHODS

Based on our previous research[1], we apply the finite element method to solve the Poisson-Nernst-Planck-Stokes equations with fully resolved electric double layers. The 2D model is computed within a 160 μm by 80 μm domain in the x-z plane, as depicted in Figure S10. When 5% H_2O_2 triggers chemical reactions on the motor surface, we assume that the proton fluxes on the anode and cathode hemispheres are in opposite directions, resulting in a net ion flux of zero. Protons are generated at the equator of the Pt side (anode) and absorbed at the poles of the Pt side (cathode),[2] as shown in Figure S11. The charged wall disturbs the upper and lower equilibrium of the physical fields generated by the motor.

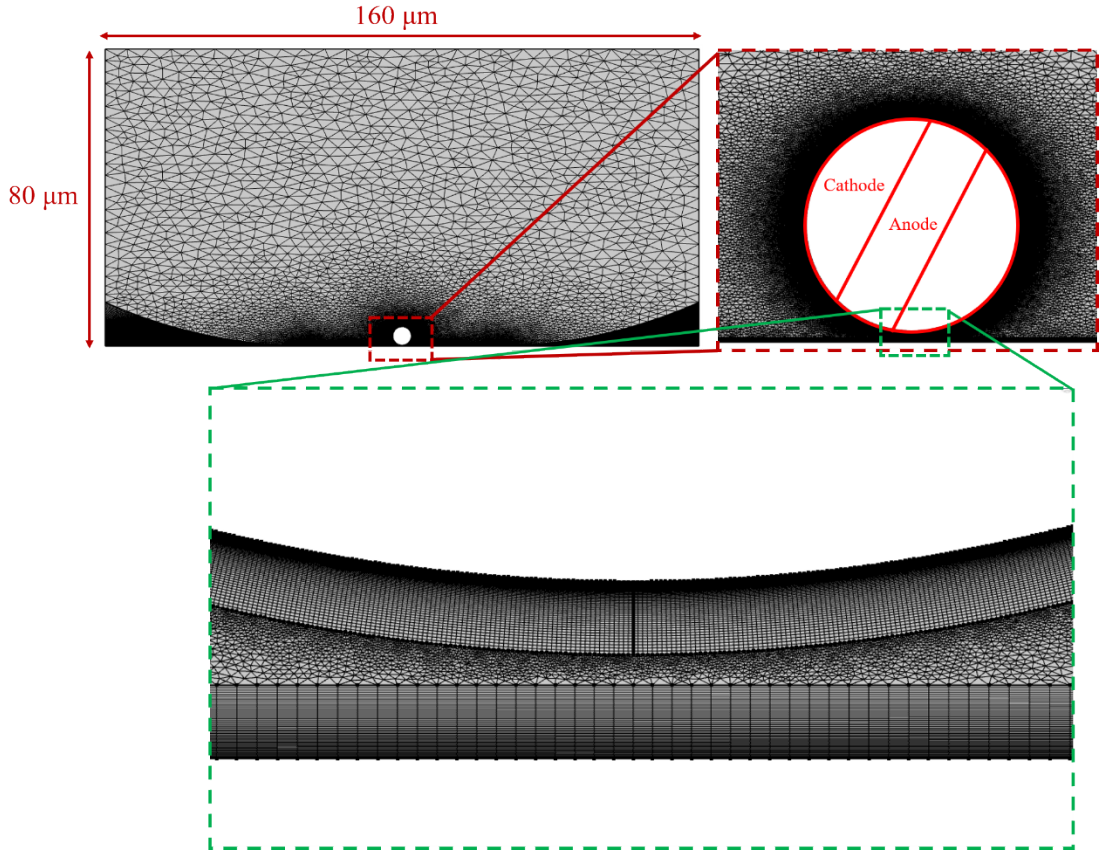

Figure S10. Schematic of the geometric setup of the model

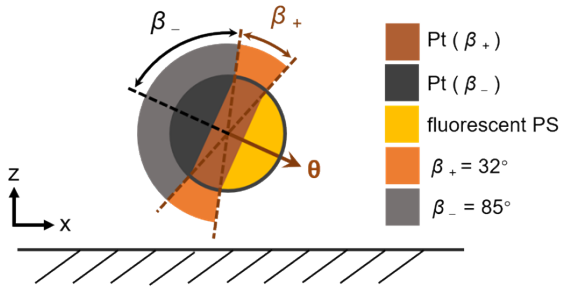

Figure S11. Schematic of the model β range setting

Our model accounts for an electrolyte containing equal concentrations of H^+ and OH^- ions, along with background ions, denoted as BI^+ and BI^-, which are included to modify the ionic strength and Debye length. With the Debye length set to 70 nm, the equilibrium height of the motors is approximately 0.27 μm, aligning closely with the experimentally measured equilibrium height.[3]

In the limit of dilute solutions, the steady-state ion concentration distribution c_i for the i-th ion is governed by the Nernst-Planck equation:

$$\nabla \cdot \mathbf{J}_i = 0 \tag{1}$$

$$\mathbf{J}_i = -D_i \nabla c_i - z_i F v_i c_i \nabla \phi \tag{2}$$

where $\mathbf{J}_i$ represents the ion flux, D_i is the diffusivity, v_i is the ion mobility, z_i is the ion valence, F is Faraday's constant, and ϕ is the electrostatic potential. The subscript $i = 1$ corresponds to H^+.

The electrostatic potential ϕ is determined by the local free charge density, as described by the Poisson equation:

$$-\varepsilon_0 \varepsilon_r \nabla^2 \phi = \rho_e \tag{3}$$

$$\rho_e = F \sum zici \tag{4}$$

where ρ_e is the local free charge density, ε_0 is the vacuum permittivity, and ε_r is the relative permittivity of the solution.

The flow field $\mathbf{u}$ is described by the Stokes equation:

$$-\nabla p + \eta \nabla^2 \mathbf{u} - \rho_e \nabla \phi = 0 \tag{5}$$

$$\nabla \cdot \mathbf{u} = 0 \tag{6}$$

where p is the pressure and $\rho_e \nabla \phi$ represents the electrical body force resulting from the coupling between the charge density and the electric field.

Chemical reactions are modeled using boundary conditions that define the molar proton fluxes on the motor surface. The motor has a uniform zeta potential, $\phi = \zeta_m$, and moves parallel to the bottom wall with a velocity V. The boundary conditions on the motor surface are as follows:

$$\mathbf{n} \cdot \mathbf{J}_{i,\text{cathode}} = -J\delta_{i,1} \quad \text{if} \quad -\beta_- < \beta < \beta_- \tag{7}$$

$$\mathbf{n} \cdot \mathbf{J}_{i,\text{anode}} = J_a \delta_{\text{i},1} \quad \text{if} \quad -\beta_- - \beta_+ < \beta < -\beta_- \text{ or } \beta_- < \beta < \beta_- + \beta_+ \tag{8}$$

$$\text{n} \cdot \mathbf{J}_i = 0 \quad \text{otherwise} \tag{9}$$

$$\phi = \zeta_m \tag{10}$$

$$\mathbf{u} = \text{Ve}_x \tag{11}$$

where β is the azimuthal angle as defined in the Figure S11, and β_+ and β_- represent the anode and cathode regions, respectively. The proton flux on the anode, J_a, is set to $J\beta_-/\beta_+$, ensuring that the net ion flux is zero. In the calculation, we set $\beta_+ = 32°$ and $\beta_- = 85°$.

At the wall, the chemical fluxes are zero, the zeta potential is $\phi = \zeta_w$, and the no-slip boundary condition is applied:

$$\mathbf{n} \cdot \mathbf{J}_i = 0 \tag{12}$$

$$\phi = \zeta_w \tag{13}$$

$$\mathbf{u} = 0 \tag{14}$$

The hydrodynamic stress tensor σ_H and the Maxwell stress tensor σ_E are derived from the physical fields as:

$$\sigma_{\text{H}} = p\mathbf{I} + \eta(\nabla \mathbf{u} + (\nabla \mathbf{u})^T) \tag{15}$$

$$\sigma_{\text{E}} = \varepsilon(\mathbf{EE} - \frac{E^2}{2}\mathbf{I}) \tag{16}$$

where $\mathbf{E}$ is the electric field and $\mathbf{I}$ is the identity matrix. The force and torque exerted on the motor

due to the chemical reaction are calculated as:

$$F_x = \mathbf{e}_x \cdot \oint_{\text{motor}} (\sigma_E + \sigma_H) \cdot \mathrm{d}\mathbf{S} \tag{16}$$

$$F_z = \mathbf{e}_z \cdot \oint_{\text{motor}} (\sigma_E + \sigma_H) \cdot \mathrm{d}\mathbf{S} \tag{16}$$

$$T_y = \oint_{\text{motor}} (\boldsymbol{r} - r_0) \times (\sigma_E + \sigma_H) \cdot \mathrm{d}\mathbf{S} \tag{16}$$

where $\boldsymbol{r}$ represents points on the motor surface, $\boldsymbol{r_0}$ is the center of the motor, and $\mathrm{d}\mathbf{S}$ is the surface element with unit normal vector $\mathbf{n}$.

The total force and torque applied to the motor is given by:

$$F_{\text{tot},x} = F_x \tag{12}$$

$$F_{\text{tot},z} = F_z - F_g \tag{13}$$

$$T_{\text{tot}} = T_y - T_g \cos\theta \tag{14}$$

In this steady-state model, the total force and torque are set to zero. The 5 μm motor moves near a charged wall at a constant self-propelling speed V, with a tilt angle θ and a height h. We use an iterative method[1] to satisfy these balance conditions, resulting in typical motor parameters near the wall: θ = 11.5°, h = 0.27 μm, and V = 3.1 μm/s. When a specific parameter is queried, the other balance parameters are fixed.

Unless stated otherwise, the parameters used in this study are listed in Table S1. The zeta potentials ζ_m, ζ_w, and flux values are determined based on Refs.[4-7], with the proton flux further adjusted to match the experimental self-propelling speed. The diffusivities of background ions BI^+ and BI^- are assumed to be the same as those of K^+ and Cl^-. The bulk concentration $c_{\text{bulk,i}}$ is determined by the Debye length, which is estimated from the motor height.

We also present the physical fields around the motor at steady-state. In Figure S12, we plot spatial distributions of protons concentration c_1^*, the electric potential ϕ^* and flow field $\mathbf{u}$ around a sliding motor. For clarity, we remove the sharp changes of fields in the Debye layer by subtracting background fields in the absence of chemical reactions from instantaneous fields, noted with asterisk superscript.

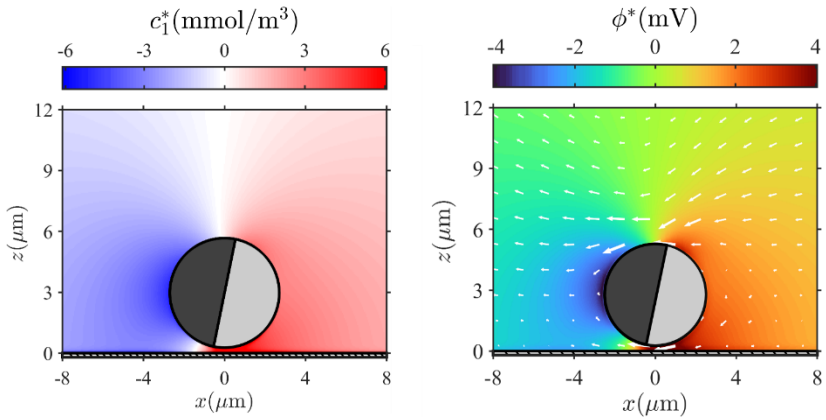

Figure S12. Instantaneous fields of hydrogen ion concentration c_1^* and electric potential ϕ^* around a Janus motor near a flat wall. These fields represent the values after subtracting those obtained in the absence of proton flux. The white arrows indicate the distribution of the fluid flow field.

Table S1. Parameters used for COMSOL modeling.

parameter	value	parameter	value
r	2.5 μm	T	293.15 K
ζ_w	-0.05 V	η	1.003×10^{-3} Pa·s
ζ_m	-0.04 V	$z_{1,3}$	1
ε_0	8.85×10^{-12} C/(V·m)	$z_{2,4}$	-1
ε_r	80	D_1	9.31×10^{-9} m^2/s
β_-	85°	D_2	5.03×10^{-9} m^2/s
β_+	32°	D_3	1.957×10^{-9} m^2/s
J	2.0×10^{-5} mol/(m^2·s)	D_4	2.032×10^{-9} m^2/s
F_g	0.16 pN	$c_{\text{bulk }1,2}$	3.5×10^{-6} mol/L
T_g	1.0 pN×μm	$c_{\text{bulk }3,4}$	1.6×10^{-5} mol/L

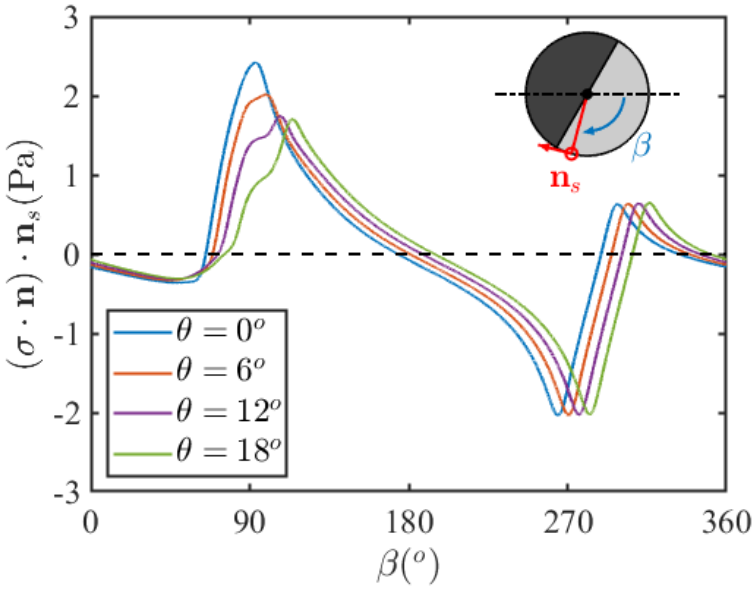

Figure S13. Hydrodynamic stress calculated at different points of a Pt Janus colloid for different tilt angles. The tangential hydrodynamic stress $\sigma\cdot\mathbf{n}_s$ is calculated as a function of azimuthal angle (β, see inset for definition), where the unit tangential vector is defined as $\mathbf{n}_s$=(−sinβ, −cosβ), following a clockwise positive convention. The results reveal that electroosmotic flow stress near the boundary (β ≈ 90°) significantly decreases as the active colloid tilts its PS cap toward the wall (i.e. increasing θ), whereas the stress on the opposite side (β ≈ 270°) remains largely unaffected. Consequently, T_A decreases with increasing tilt angle and eventually becomes negative, explaining the observed sign change around θ ≈ 13–14° in Figure 4b in the main text.

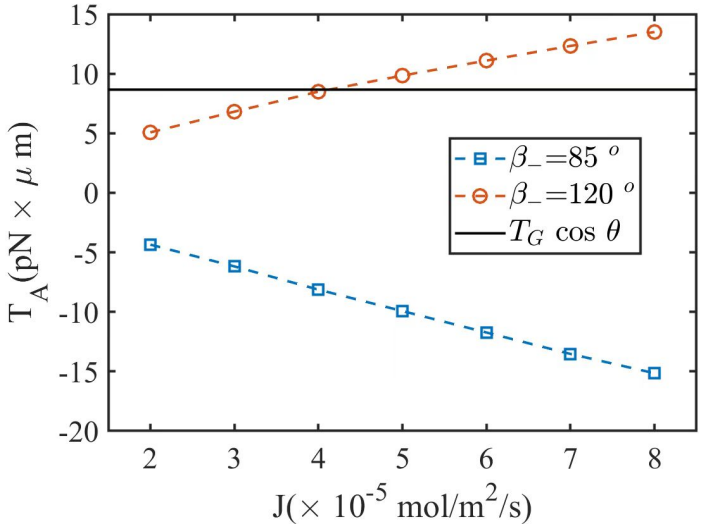

Figure S14. Activity-induced torque (T_A) values simulated for different chemical flux on the Pt cap (J) at two cap coverage values (β_-, the azimuthal angle for the cathodic part of the Pt cap, see Fig. S11 for definition). The θ of the sphere is fixed at 30°, which is a large value specifically chosen to find the simulation parameters necessary to allow such a large tilt. The results show that T_A values calculated at β_-=85° are increasingly negatively at increasing J, so that a steady state θ where $T_A+T_G=0$ cannot be found. Rather, increasing β_-=120° reversed the sign of T_A and a steady state θ is found at J=~4×10^{-5} mol/(m^2·s). The values of β_+ are the same for these two cases.

Reference

(1) Xu, Y.; Liu, C.; Liu, J.; Xu, P.; Xiao, Z.; Wang, W.; Zhang, H. P. Measuring Attractive Interaction between a Self-Electrophoretic Micromotor and a Wall. *Physical Review Letters* **2024**, *133* (25), 258304. DOI: 10.1103/PhysRevLett.133.258304.

(2) Lyu, X.; Liu, X.; Zhou, C.; Duan, S.; Xu, P.; Dai, J.; Chen, X.; Peng, Y.; Cui, D.; Tang, J.; et al. Active, Yet Little Mobility: Asymmetric Decomposition of H2O2 Is Not Sufficient in Propelling Catalytic Micromotors. *Journal of the American Chemical Society* **2021**, *143* (31), 12154-12164. DOI: 10.1021/jacs.1c04501.

(3) Ketzetzi, S.; de Graaf, J.; Kraft, D. J. Diffusion-Based Height Analysis Reveals Robust Microswimmer-Wall Separation. *Physical Review Letters* **2020**, *125* (23), 238001. DOI: 10.1103/PhysRevLett.125.238001.

(4) Wang, W.; Chiang, T.-Y.; Velegol, D.; Mallouk, T. E. Understanding the Efficiency of Autonomous Nano- and Microscale Motors. *Journal of the American Chemical Society* **2013**, *135* (28), 10557-10565. DOI: 10.1021/ja405135f.

(5) Moran, J. L.; Wheat, P. M.; Posner, J. D. Locomotion of electrocatalytic nanomotors due to reaction induced charge autoelectrophoresis. *Physical Review E* **2010**, *81* (6), 065302. DOI: 10.1103/PhysRevE.81.065302.

(6) Dougherty, G. M.; Rose, K. A.; Tok, J. B.-H.; Pannu, S. S.; Chuang, F. Y. S.; Sha, M. Y.; Chakarova, G.; Penn, S. G. The zeta potential of surface-functionalized metallic nanorod particles in aqueous solution. *ELECTROPHORESIS* **2008**, *29* (5), 1131-1139. DOI: https://doi.org/10.1002/elps.200700448.

(7) Liu, C.; Zhou, C.; Wang, W.; Zhang, H. P. Bimetallic Microswimmers Speed Up in Confining

Channels. *Physical Review Letters* **2016**, *117* (19), 198001. DOI: 10.1103/PhysRevLett.117.198001.